

Thermophysical properties of the α - β - γ polymorphs of Mg_2SiO_4 : a computational study

G. Ottonello · B. Civalleri · J. Ganguly ·
M. Vetuschi Zuccolini · Y. Noel

Received: 17 December 2007 / Accepted: 7 August 2008
© Springer-Verlag 2008

Abstract Thermophysical properties of the various polymorphs (i.e. α -, β - and γ) of Mg_2SiO_4 were computed with the CRYSTAL06 code within the framework of CO-LCAO-GTF approach by using the hybrid B3LYP density functional method. Potential wells were calculated through a symmetry preserving, variable cell-shape structure relaxation procedure. Vibrational frequencies were computed at the long-wavelength limit corresponding to the center of the Brillouin zone ($\mathbf{k} \rightarrow 0$). Thermodynamic properties were estimated through a semiclassical approach that combines B3LYP vibrational frequencies for optic modes and the Kieffer's model for the dispersion relation of acoustic modes. All computed values except volume (i.e. electronic energy, zero point energy, optical vibrational modes, thermal corrections to internal energy, standard state enthalpy and Gibbs free energy of reaction, bulk

modulus and its P and T derivatives, entropy, C_V , C_P) are consistent with available experimental data and/or reasonable estimates. Volumes are slightly overestimated relative to those determined directly by X-ray diffraction. A set of optimized volumetric properties that are consistent with the other semiclassical properties of the phases α , β and γ have been derived by optimization procedure such that the calculated boundaries for the α/β and β/γ equilibria have the best overall agreement with the experimental data for these transitions.

Keywords Polymorphic transitions · Thermodynamic properties · Forsterite · Wadsleyite · Ringwoodite

Electronic supplementary material The online version of this article (doi:10.1007/s00269-008-0260-4) contains supplementary material, which is available to authorized users.

G. Ottonello (✉) · M. Vetuschi Zuccolini
Laboratorio di Geochimica at DIPTERIS, Università di Genova,
Corso Europa 26, 16132 Genova, Italy
e-mail: giotto@dipteris.unige.it

B. Civalleri
Dipartimento di Chimica IFM and NIS Centre of Excellence,
Università di Torino, Via Giuria 7, 10125 Torino, Italy

J. Ganguly
Department of Geosciences, University of Arizona,
Tucson, AZ 85721, USA

Y. Noel
Laboratoire de Pétrologie, Modélisation de Matériaux et
Processus, Université Pierre et Marie Curie, 4, Place Jussieu,
75252 Paris Cedex 05, France

Introduction

The thermodynamic properties of mantle minerals play a central role in the understanding of phase relations in the terrestrial and planetary mantles, their seismic properties, and their thermal and density structures that influence the mantle dynamics (e.g. Saxena et al. 1993; Fabrichnaya 1999; Ganguly and Frost 2006; Ganguly et al. 2007). Over the last two decades or so, major advancements have been made in the understanding of the mineralogy of the terrestrial and Martian upper and lower mantle through experimental studies at very high pressure and temperature conditions in the multi-anvil apparatus and diamond cells. However, there are conditions in the Earth's mantle at which laboratory experiments are extremely difficult either because of the extreme P - T condition or very slow reaction kinetics at the thermal state of interest. An example of the latter problem is the recent study of Ganguly and Frost (2006) on the stability

of anhydrous B-phase (Anh-B) in the Earth's mantle and subducting oceanic slabs. On the basis of approximate thermodynamic properties of the phase retrieved from their high temperature experimental data, and estimated on the basis of empirical schemes, these authors predicted that in the interior of a cold subducting oceanic slab such as Tonga, the transition from the phase wadsleyite (wads: $\beta\text{-Mg}_2\text{SiO}_4$) to ringwoodite (ring: $\gamma\text{-Mg}_2\text{SiO}_4$) should proceed via an intermediate phase assemblage Anh-B + stishovite (St) (wads \rightarrow Anh-B + St \rightarrow ring), leading to eye-shaped splitting of the seismic wave velocities. However, the temperature condition for experimental verification of this prediction is deemed too low for the achievement of detectable extent of reaction within reasonable laboratory time scales in a multi-anvil apparatus. This and other problems relating to mantle phase equilibria call for computational thermodynamic approach for which one needs reliable thermodynamic data base.

While self-consistent thermodynamic data base such as those of Berman (1988), Johnson et al. (1992), Holland and Powell (1990) have been widely used in the computation of metamorphic phase equilibria, these are not suitable for problems related to the deep mantle of the Earth. Saxena et al. (1993) and Fabrichnaya et al. (2004) have developed internally consistent data bases for the mantle minerals at low to high P - T conditions from the available phase equilibrium and calorimetric data, but these do not have the properties of many of the mantle minerals for the lack of adequate experimental data from which to retrieve the thermodynamic properties. To circumvent this type of problem, a number of workers have made major efforts to determine the thermodynamic properties from quantum mechanical calculations (e.g. Cohen 1991; Karki and Crain 1998; Panero et al. 2006; Yu and Wentzcovitch 2006; Li et al. 2007; Wu and Wentzcovitch 2007). In this paper, we report part of our attempt in the realm of ab initio quantum mechanical calculations of the thermo-chemical and thermo-physical properties of mantle minerals. This contribution is mainly devoted to an appraisal of the accuracy that could be achieved by a computational approach to determine the univariant equilibrium boundaries for the mineralogical reactions in the Earth's mantle (other forthcoming contributions concern the thermophysical properties of stishovite and AnhB). Thermodynamic data for all these phases are needed to determine the P - T stability field of the Anh-B + St through first principles. Moreover, the different polymorphs of Mg_2SiO_4 constitute the most abundant minerals in the Earth's upper mantle and Martian mantle (Fei and Bertka 1999). Although there are several studies on the thermodynamic properties of these minerals utilizing phase equilibrium and calorimetric data, there are also significant disagreements. Our computed results would be helpful in sorting out these problems.

Computational details

Computations have been carried out with a developmental version of the CRYSTAL06 program (Dovesi et al. 2006). All-electron calculations were performed within the linear combination of atomic orbitals (LCAO) approach with the hybrid B3LYP functional (Becke 1993; Stephens et al. 1994), which contains a hybrid HF and density functional exchange-correlation functional, composed of the Becke three-parameter exchange functional and the LYP (Lee et al. 1988) correlation functional. The all-electron Gaussian-type basis set adopted is a 8-511G(d) for magnesium (Pascale et al. 2005), a 88-31G(d) set for silicon and a 8-411G(d) set for oxygen (Nada et al. 1996) (see Appendix A for more details).

Cut-off limits in the evaluation of Coulomb and exchange series appearing in the SCF equation for periodic systems were set to 10^{-6} for coulomb overlap tolerance, 10^{-6} for coulomb penetration tolerance, 10^{-6} for exchange overlap tolerance, 10^{-6} for exchange pseudo-overlap in the direct space, and 10^{-12} for exchange pseudo overlap in the reciprocal space (see Saunders et al. 2003). The density functional theory (DFT) exchange-correlation contribution is evaluated by numerical integration over the cell volume (Pascale et al. 2004a, b). In the present work, we used a (75,434)p grid that contains 75 radial points and a variable number of angular points, with a maximum of 434 on the Lebedev surface in the most accurate integration region (see Appendix A for further details). The condition for the SCF convergence was set to 10^{-7} a.u. on the total energy difference between two subsequent cycles. The reciprocal space is sampled according to a regular sublattice with a shrinking factor IS equal to four corresponding to 27, 18 and 8 k-points in the sampling of the irreducible Brillouin zone (Dovesi et al. 2006) for α -, β - and γ - Mg_2SiO_4 polymorphs, respectively. The gradients with respect to atomic coordinates and lattice parameters are evaluated analytically (Doll 2001; Doll et al. 2001, 2004). The equilibrium structure is determined (Civalleri et al. 2001) by using a quasi-Newton algorithm with a BFGS Hessian updating scheme and following geometry optimization strategy as proposed by Schlegel (1982). Convergence in the geometry optimization process is tested on the root-mean-square (RMS) and the absolute value of the largest component of both the gradients and nuclear displacements. For all atoms, the thresholds for the maximum and the RMS forces have been set to 0.00045 and 0.00030 a.u., and those for the maximum and the RMS atomic displacements to 0.00180 and 0.00120 a.u., respectively.

The potential wells of the phases were calculated by a symmetry preserving, variable cell-shape structure relaxation procedure and fitted to a third order finite-strain equation.

Regarding the calculation of frequencies, we refer to a previous paper (Pascale et al. 2004a, b) for the methodological details. Here, we simply recall that within the harmonic approximation, frequencies at the Γ point ($\mathbf{k} = 0$) are obtained by diagonalizing the mass-weighted Hessian matrix W , whose (i,j) element is defined as $W_{ij} = H_{ij}/(M_i M_j)^{1/2}$, where H_{ij} is the Hessian matrix of the second derivatives of the energy with respect to the atomic positions and M_i and M_j are the masses of the atoms associated with the i and j coordinates, respectively. In the program CRYSTAL, energy first derivatives are calculated analytically, while second derivatives are evaluated numerically using a two-point or three-point formula. For the vibrational frequencies calculation, the tolerance on the energy convergence of the SCF cycles was set to 10^{-10} a.u.

At the long-wavelength limit corresponding to the center of the Brillouin zone ($\mathbf{k} \rightarrow 0$), the first three solutions of the dispersion relation vanish. The dispersion relation is given by

$$\omega = \omega_i(k) \quad 1 \leq i \leq 3n \quad (1)$$

where ω is the angular frequency and n is the number of atoms in the unit cell (Born and Huang 1954). For the thermal analysis the first three (acoustic) vibrational modes are here treated according to a semiempirical model based on sound wave dispersion (Kieffer 1979a, b), and coupled with the ab initio calculated vibrational frequencies of the remaining $3n-3$ modes. Therefore, our procedure is not fully ab initio and will be denoted hereafter as *semiclassical*. Further details are presented in the following sections.

Static calculations

Forsterite (α -Mg₂SiO₄)

Forsterite, the α polymorph of the Mg-orthosilicate, crystallizes in the orthorhombic bipyramidal class (space group *Pbnm*; non-conventional setting of *Pnma* n. 62). There are six irreducible atoms in the conventional cell and 28 atoms in the unit-cell (four formula units per unit cell). Since it is the most abundant mineral in the Earth's upper mantle, forsterite has been subjected to numerous investigations by mineralogists and crystallographers (e.g. Bragg and Brown 1926; Cernik et al. 1990; Belov et al. 1951; Baur 1972; Smyth and Hazen 1973; Hazen 1976; Fujino et al. 1981; Lager et al. 1981; Kudoh and Takeuchi 1985; van der Wal et al. 1987; Della Giusta et al. 1990). The first structural refinement of forsterite was carried out by Bragg and Brown (1926). First-principles investigations of forsterite dealt mainly with the elastic and structural properties at high pressure (Jochym et al. 2004; Brodholt

et al. 1996; Da Silva et al. 1997), and it is only recently that the vibrational behavior of the mineral has been investigated by first-principles (Noel et al. 2006; Li et al. 2007). The variational structure at the athermal limit in the absence of external pressure was obtained by full geometry optimization of both lattice parameters and atomic positions. The resulting volume at the athermal limit, V° , is 4.4682 J/bar ($a_0 = 4.794$ Å; $b_0 = 10.294$ Å; $c_0 = 6.013$ Å; $V_0 = 296.7$ Å³) with a B3LYP total energy (gfw basis), E_{B3LYP} , of -991.055720 hartree (1 hartree = 1 atomic unit = 2625.5 kJ/mol). These results are very similar to those obtained at the B3LYP level of theory by Noel et al. (2006) with a slightly different basis set. In the present work, a slightly larger b_0 cell edge (10.29 against 10.25 Å) is obtained. Computed static volume is close to other computed results (see Table 1) obtained at both LDA (Haiber et al. 1997; Li et al. 2007) and GGA (Jochym et al. 2004) level of theory with the B3LYP volume being intermediate between the two sets of values.

Data from the detailed experimental compressional studies by Hazen (1976) up to 5 GPa at ambient T , coupled with guessed values of thermal expansion from the athermal limit to ambient T , allowed us to assign provisional cell edges to each compressional state and to refine minimum energy c/b and a/b ratios over a wide P range at the athermal limit. This procedure, generally known as “*symmetry preserving, variable cell-shape structure relaxation*” (Kiefer et al. 2001; Wentzcovitch et al. 1993; da Silva et al. 1997; Karki et al. 1997) was computationally very demanding because 152 runs (86 for the c/b ratios and 66 for the a/b ratios) were necessary to determine satisfactorily the potential well of the substance on 14 different compressional states.

The results of the iterative computations are presented as electronic supplementary material in Figs. S1 and S2 (supplementary materials), to illustrate the internal consistency of the procedure. In Fig. S1 (supplementary material) we show the local minima on the various c/b curves for different nominal pressures. In Fig. S2 (supplementary material) we show the optimized values of the a/b ratio (local minima) that are determined on the basis of the previously optimized c/b ratios and the molar volumes corresponding to the nominal input pressure.

The partial derivative of a third-order polynomial fitted over the molar B3LYP total energy (E_{B3LYP} , J/mole)–molar volume (V , J/bar) couples allowed us to establish the ab initio potential value of static pressure P_{st} corresponding to a given compressional state, which is shown by a number on the various $E = f(a/b)$ curves in Fig. S2 (supplementary material).

The calculated ratios of a/b cell edges versus the computed static pressure show good agreement with the available experimental data, while those of c/b cell edges are found to

Table 1 Equation of State parameters of forsterite

| V_0 (Å ³) | K_0 (GPa) | K' | References |
|-------------------------|-------------|-------|--|
| Calculated | | | |
| 296.7 | 130.8 | 4.001 | <i>This study (static)</i> |
| 297.5 | 125.6 | 4.001 | <i>This study (298.15 K)</i> |
| 290.1 | 134.6 | 5.2 | Saxena et al. (1993) |
| 291.9 | | | Guyot et al. (1996) (300 K) |
| 293.3 | 137.0 | 3.75 | Haiber et al. (1997) (static) |
| 298.8 | | | Jochym et al. (2004) (static) |
| 286.2 | 134.8 | 4.74 | Jacobs et al. (2006) (static) |
| 288.8 | | | Jacobs et al. (2006) (298.15 K) |
| 289.5 | 126.4 | 4.2 | Li et al. (2007) (300 K) |
| Experimental | | | |
| | 127.4 | 4.8 | Meng et al. (1993) |
| | | 4.4 | Li et al. (1996) |
| | | 5.2 | Zha et al. (1996) |
| 290.3 | | | Smyth and Hazen (1973) (296 K) |
| 289.8 | | | Hazen (1976) |
| 289.6 | | | Fujino et al. (1981) |
| 285.5 | | | Baur (1972) |
| 290.0 | | | Lager et al. (1981) |
| 292.3 | | | Bragg and Brown (1926), Belov et al. (1951) |
| 290.2 | | | van der Wal et al. (1987) |
| 290.3 | | | Cernik et al. (1990); Della Giusta et al. (1990) |
| | 128 | | Isaak (1991) (static, extrapolated) |
| | 134.6 | | Anderson (1995) (static, extrapolated) |
| | 126 | | Manghnani and Matsui (1981) (static, extrapolated) |
| 290.1 | 125 | 4.0 | Downs et al. (1996) (300 K) |

be somewhat smaller than that determined experimentally [Fig. S3 (supplementary material)]. It should be noted, however, that there is some disagreement in the literature about the optimum a/b and c/b ratios at ambient conditions. In spite of these minor problems, our results (ab initio cell edges vs. ab initio static pressure) are mostly consistent with the experimental data of Hazen (1976) at high pressure (Fig. 1). We find Mg-olivine to compress anisotropically, and preferentially along the b axis.

The bulk modulus of the mineral at zero pressure ($K_0 = 130.810$ GPa) and its P -derivative ($\partial K/\partial P = K' = 4.001$) were obtained by Gaussian integration of the Birch–Murnaghan third order finite strain isothermal equation of state (EoS):

$$P_{\text{st}} = -\left(\frac{\partial E_{\text{ai}}}{\partial V}\right)_{T=0} = \frac{3}{2}K_0 \left[\eta^{-7/3} - \eta^{-5/3} \right] \times \left\{ 1 - \frac{3}{4}(4 - K') \left[\eta^{-2/3} - 1 \right] \right\} + P_0 \quad (2)$$

where η is a dimensionless variable, often called the “dilatation” parameter, and defined as $\eta = V/V_0$, with V_0 being the volume at the reference pressure P_0 . According to Anderson (1995), the value of the bulk modulus at the athermal limit is

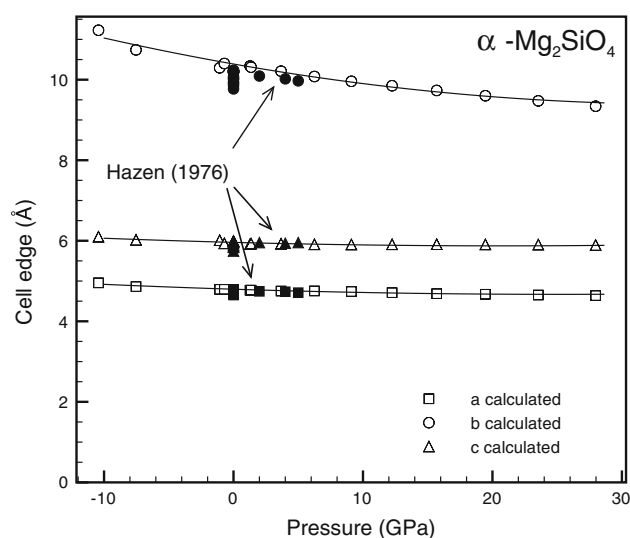


Fig. 1 Cell edges of α -Mg₂SiO₄ (Å) versus pressure (GPa). Computed results of this study (*open symbols*) are compared with the experimental data of Hazen (1976) (*filled symbols*)

intermediate between the value given by Isaak (1991) (128 GPa) and that obtained by a linear extrapolation to the athermal limit of the experimental compressibility data at

$P = 0$ ($K_0 = 134.6$ GPa; cf. Anderson et al. 1992 and Figure 2.4 and Table A-7.5 in Anderson 1995). The pressure derivative of the bulk modulus at the athermal limit, K' , is at the lower end of literature estimates, which range from 4.0 to 5.2 (Downs et al. 1996; Li et al. 1996; Sumino et al. 1977; Sumino and Anderson 1984; Zha et al. 1996). A first sight inspection to Fig. S4 (supplementary material) could suggest that the wide range of K' is ascribable to the fact that a finite strain third order equation is inadequate to describe accurately the static potential well over a wide P -range. However, the pressure derivative of the bulk modulus at the athermal limit is very near to the condition ($K' = 4$) that reduces the Birch–Murnaghan expansion to second order (see also Anderson 1995, to this purpose). Indeed $K' = 4$ was adopted by Downs et al. (1996) to retrieve their experimental data in the P range 0–17.2 GPa. It is thus not appropriate to explore higher order equations such as the Vinet EoS or the fourth order Birch–Murnaghan. In Fig. 2, we see that our predicted V/V_0 ratios are not far from the experimental observations of Downs et al. (1996) within the range of extrinsic stability of the polymorph. The agreement is rather good also with the computational results of Li et al. (1996) while the thermodynamic assessments of Saxena et al. (1993) and Jacobs et al. (2006) suggest a lower isothermal compressibility of the polymorph at all P of interest, in line with the experiments of Will et al. (1986).

The results of our static calculations are summarized, and compared with the current estimates and experimental data in Table 1.

Wadsleyite (β -Mg₂SiO₄)

Wadsleyite, which is also referred to as “beta form” or “modified spinel” in the literature, is an orthorhombic

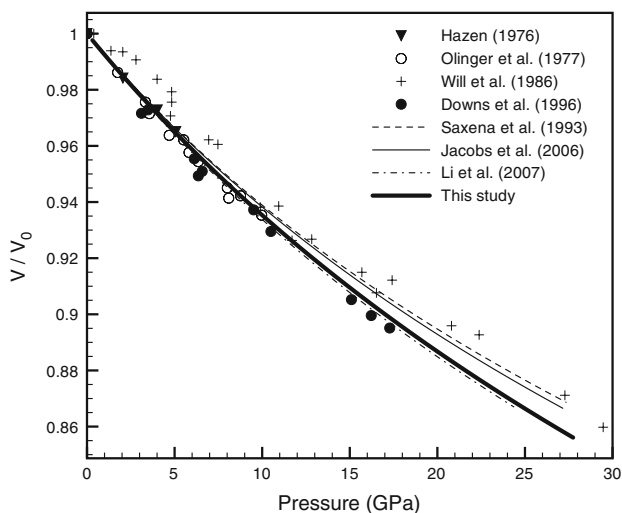


Fig. 2 Compressional states of forsterite at various P conditions. Computational results are compared with experiments and estimates

bipyramidal ($Ibmm$) polymorph of the Mg-orthosilicate. There are six irreducible atoms in the conventional cell. Canonical structure was refined long ago by Moore and Smith (1970) and Baur (1972). The results of the detailed experimental compressional studies (Hazen et al. 2000; Li et al. 1998), in situ high P – T measurements (Meng et al. 1993) and previous first-principles investigations (Haiber et al. 1997; Kiefer et al. 2001; Wu and Wentzcovitch 2007) allowed us to assign provisional cell edges to each compressional state and to refine minimum energy c/b and a/b ratios over a wide pressure range at the athermal limit, as described above for the α polymorph.

The partial derivative of a third-order polynomial fitted to the calculated molar total energy (E_{B3LYP} , J/mole)—molar volume (V , J/bar) couples allowed us to establish the ab initio potential value of static pressure, P_{st} . As illustrated in Fig. 3, our computed results are consistent with the experimental data of Hazen et al. (2000). The mineral compresses anisotropically and preferentially along the c axis. The c/b and a/b ratios gradually converge at high pressure while the a/b ratio remains fairly constant.

Setting the nominal static pressure to zero at the athermal limit, we estimated a cell volume of 550.0 Å³ ($a_0 = 5.731$ Å; $b_0 = 11.516$ Å; $c_0 = 8.333$ Å). A complete optimization of the crystalline structure gave $V^0 = 550.4$ Å³ ($a_0 = 5.734$ Å; $b_0 = 11.521$ Å; $c_0 = 8.332$ Å) and a B3LYP total energy (gfw basis) $E_{B3LYP} = -991.0427538$ hartree. As for forsterite, the predicted volumes are slightly larger than the one reported from calculations at the LDA level of theory (Haiber et al. 1997; Kiefer et al. 2001; Wu and Wentzcovitch 2007).

The bulk modulus of the substance at zero pressure ($K_0 = 161.826$ GPa) and its pressure derivative

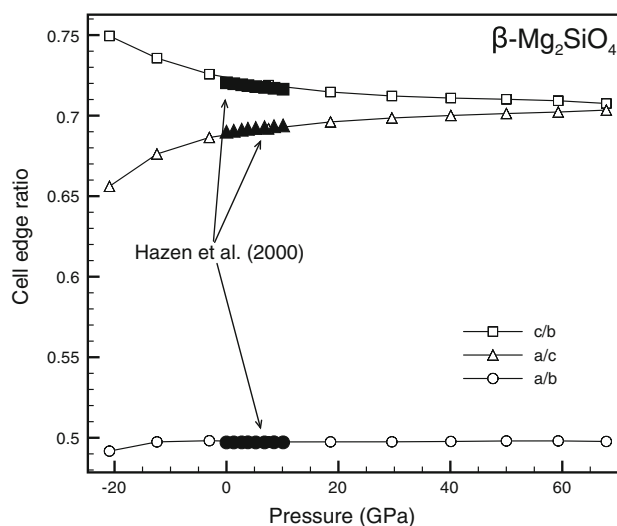


Fig. 3 Cell edge ratios of β -Mg₂SiO₄ (adimensional) versus pressure (GPa). Results of this study are compared with the experiments of Hazen et al. (2000)

($\partial K/\partial P = K' = 4.415$) were obtained by Gaussian integration of the Birch–Murnaghan third order finite strain isothermal EoS and are consistent with the room-temperature estimates of Akaogi et al. (1989) based on the data of Sawamoto et al. (1984) and Tanaka et al. (1987) (i.e. $K_T = 173$; $K' = 4.3$). As shown in Fig. S5 (supplementary material), the Birch–Murnaghan equation provides for this phase a good fit of the computed energies. The results of our static calculations are compared in Table 2 with those of other static calculations and experimental data.

Ringwoodite (γ -Mg₂SiO₄)

The γ -polymorph, which is also known as ringwoodite, crystallizes in the cubic system (crystal class Cubic Hexakisoctahedral, Space Group $Fd\bar{3}m$). There are 14 atoms in the unit cell and three irreducible atoms in the conventional cell. Only oxygen is in general position. Based on the ab initio molecular dynamics investigation of Haiber et al. (1997), we assigned provisional cell edge (a_0) and oxygen fractional coordinate (x) in a wide pressure range, from a nominally negative pressure of -40 GPa (corresponding to a virtual expanded state) to 110 GPa. For each pressure condition (and corresponding cell edge), the fractional coordinates of oxygen (x) were varied within the range ± 0.003 of the initially assigned value to account for the effect of internal strain on the electronic energy of the substance [Fig. S6 (supplementary material)]. A geometry optimization on each selected (a_0, x) couple allowed us to

further relax the internal coordinates and to determine the potential well of the substance.

On the basis of the partial derivative of a third-order polynomial fitted over 17 molar B3LYP total energy (E_{B3LYP} , J/mole)—molar volume (V , J/bar) couples, we established the ab initio potential value of static pressure, P_{st} , corresponding to each selected (a_0, x) [see also Fig. S6 (supplementary material)] and located the zero pressure condition. The resulting molar volume V° is 3.9967 (J/bar) ($a_0 = 8.0975$ Å) at the athermal limit. A final geometry optimization on the conformed minimum ($a_0 = 8.097477$ Å, $x = 0.244678$) resulted in a B3LYP total energy (gfw basis) $E_{\text{B3LYP}} = -991.037853$ hartree.

Our results are in overall agreement with the first principles computations. Again, B3LYP volumes are intermediate between LDA (Haiber et al. 1997; Kiefer et al. 1999; Yu and Wentzcovitch 2006) and GGA (Piekarz et al. 2002) data. However, when compared with the available experimental data (Hazen et al. 1993; Weidner et al. 1984; Ridgen and Jackson 1991), all ab initio computations seem to overestimate the cell edge of ringwoodite for pressures up to ~ 60 GPa and to underestimate it at higher pressures (Fig. 4).

In Table 3, our computed results are compared with previous calculations and experimental data. Application of the Birch–Murnaghan equation through non-linear minimization indicates a zero point bulk modulus $K_0 = 196.389$ GPa, roughly consistent with the extrapolation to the athermal limit of the experimental values

Table 2 Equation of State parameters for wadsleyite

| V_0 (Å ³) | K_0 (GPa) | K' | References |
|-------------------------|-------------|-------|---------------------------------------|
| Calculated | | | |
| 550.4 | 161.8 | 4.415 | <i>This study (static)</i> |
| 551.7 | 158.6 | 4.415 | <i>This study (298.15 K)</i> |
| 527.4 | 180.8 | 4.34 | Kiefer et al. (2001) (static) |
| 535.1 | 169.2 | 4.53 | Kiefer et al. (2001) (300 K) |
| 545.2 | 179.0 | 4.26 | Haiber et al. (1997) (static) |
| 538.6 | 181.4 | 4.3 | Saxena et al. (1993) |
| 528.1 | 179.2 | 4.20 | Jacobs et al. (2006) (static) |
| 533.5 | – | – | Jacobs et al. (2006) (298.15 K) |
| 541.4 | 165.7 | 4.44 | Wu and Wentzcovitch (2007) (298.15 K) |
| 537.0 | 169.7 | 4.15 | Matsui (1999) |
| Experimental | | | |
| 535.3 | 160 ± 3 | 4 | Hazen et al. (1990) |
| 539.3 | 172 ± 3 | 6.3 | Hazen et al. (2000) |
| | 172.6 | 4.8 | Meng et al. (1993) |
| 538.1 | – | – | Horiuchi and Sawamoto (1981) |
| 538.6 | – | – | Akimoto et al. (1976) |
| – | 173 | 4.3 | Akaogi et al. (1989) |
| – | 174 | 4.3 | Fei et al. (1992) |

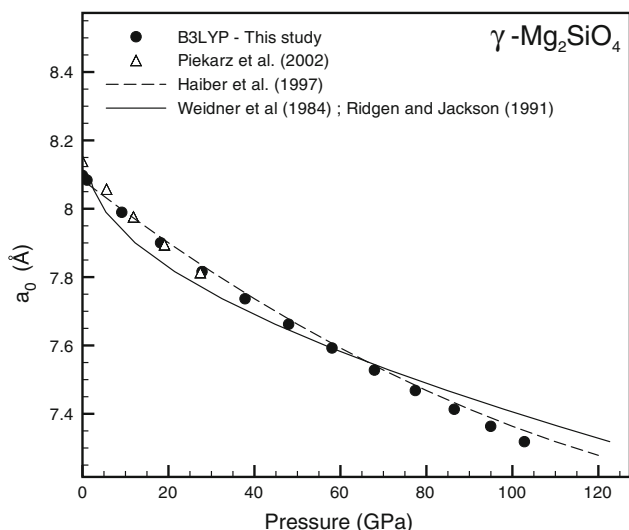


Fig. 4 Cell edge of γ -Mg₂SiO₄ (Å) versus pressure (GPa). Results of this study are compared with literature theoretical estimates and experiments

measured at room temperature by Meng et al. (1994) ($K_0 = 182$ GPa), Weidner et al. (1984) ($K_0 = 183$ GPa) and Jackson et al. (2000) ($K_0 = 185$ GPa) (Table 3), and a pressure derivative $\partial K/\partial P = K' = 4.322$, which is close to the value measured by Meng et al. (1994; $K' = 4.2$). The Birch–Murnaghan equation provides a reasonable fit of the computed energies especially at high pressure [Fig. S7 (supplementary material)].

Table S1 (supplementary material) summarizes the results of our static computations at the athermal limit for the three polymorphs of Mg₂SiO₄.

Table 3 Equation of State parameters for ringwoodite

| V_0 (Å ³) | K_0 (GPa) | K' | References |
|-------------------------|-------------|-------|---|
| Calculated | | | |
| 530.9 | 196.4 | 4.322 | This study (static) |
| 531.7 | 193.3 | 4.322 | This study (298.15 K) |
| 533.5 | 189.0 | 4.08 | Haiber et al. (1997) (static) |
| 497.0 | 206.8 | 4.0 | Kiefer et al. (1999) (static, K' assumed) |
| 526.7 | 196.9 | 4.3 | Saxena et al. (1993) |
| 539.1 | 176.0 | | Piekarz et al. (2002) (static) |
| | 189.4 | 4.33 | Jacobs et al. (2006) (static) |
| 527.5 | 184.6 | 4.5 | Yu and Wentzcovitch (2006) (300 K) |
| Experimental | | | |
| 523.9 | 190.3 | 4.1 | Meng et al. (1994) (static, extrapolated) |
| 526.7 | 182.0 | 4.2 | Meng et al. (1994) (300 K) |
| | 182.6 | 5.0 | Meng et al. (1993) (static) |
| 526.7 | – | – | Katsura and Ito (1989) (298.15 K) |
| 524.6 | – | – | Ito and Yamada (1982) |
| 526.5 | – | – | Katsura et al. (2004) (300 K) |

Vibrational calculations

Forsterite (α -Mg₂SiO₄)

There are 28 atoms in the orthorhombic bipyramidal unit cell of the α -polymorph of Mg₂SiO₄. The irreducible representation of vibrational modes, with a group theoretical treatment of the optical zone-center (Γ point; $\mathbf{k} = 0$), yields

$$\Gamma = 7B_{2g} + 14B_{2u} + 7B_{3g} + 14B_{3u} + 10A_u + 11B_{1g} + 10B_{1u} + 11A_g \quad (3)$$

In Table S2 (supplementary material) we list the vibrational frequencies obtained in this study and the results of their mode-gamma analysis. The harmonic vibrational frequencies at Γ point obtained in this study do not differ much from the results of Noel et al. (2006) and the recent work by Li et al. (2007) at the LDA level of theory within a planewave/pseudopotential theoretical approach, with the mean deviation being -5 and -10 cm⁻¹, respectively. In the same table we also report the longitudinal optical–transversal optical (LO–TO) splitting connected with induced dipole moment in polar crystals. Here, the LO–TO splitting were obtained by adding a nonanalytical term (Dovesi et al. 2006) and adopting the dielectric tensor as computed at the same level of theory by Noel et al. (2006) ($xx = 2.564$, $yy = 2.423$; $zz = 2.472$). Only B_{1u} , B_{2u} and B_{3u} modes show a significant LO–TO splitting which attains 133 cm⁻¹ in the largest case. The effect of this contribution on the vibrationally dependent thermodynamic properties is thus rather small and it was not computed for other polymorphs (see “Discussion” later on).

The quasi-harmonic mode-gamma analysis of the $\alpha_T K_T$ product¹:

$$\alpha_T K_T = \frac{R}{ZV} \sum_{i=4}^{3n} \gamma_i e^{-X_i} \left(\frac{X_i}{e^{X_i} - 1} \right)^2 \quad (4)$$

where $X_i = \frac{\hbar\omega_i}{kT}$ (with \hbar = Planck’s constant divided by 2π and k = Boltzmann’s constant) and

$$\gamma_i = - \frac{\partial \ln v_i}{\partial \ln V} \quad (5)$$

and the summation is extended to all optical modes [Table S2 (supplementary material)], shows that at high T , $\alpha_T K_T$ has a quite constant value, averaging 4.47×10^{-3} GPa/K in the T range $1,000 \leq T \leq 3,000$ K and attaining 0.0046 GPa/K at the $T \rightarrow \infty$ limit (Fig. 5; Table 4). According to Anderson (1995) the $\alpha_T K_T$ product of forsterite increases from 3.46×10^{-3} GPa/K at 300 K to 4.40×10^{-3} GPa/K at 1,700 K with roughly

¹ Note that Eq. (4) differs from the usual notation (cf. Anderson 1995) in having the term Z (number of formula units per unit cell) in the denominator.

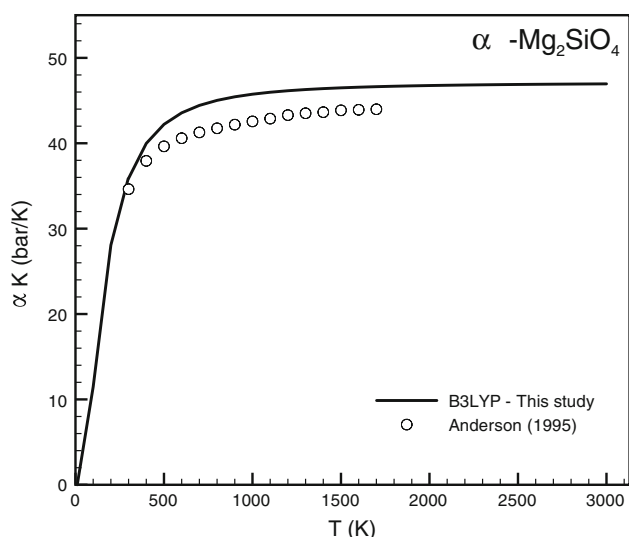


Fig. 5 Computed αK product of forsterite compared with the indications of Anderson (1995)

constant values above the Debye temperature of the substance (see Figure 2.5 and Table A–7.5 in Anderson 1995).

The quasi-harmonic treatment of vibrational frequencies allows us to establish the thermal dependency of the bulk modulus that is given by (see Anderson 1995; for a detailed treatment):

$$\left(\frac{\partial K}{\partial T}\right)_P = -(\alpha K)_\infty \times [K' - q^{\text{ht}} + 1] \quad (6)$$

where $(\alpha K)_\infty$ is the limiting αK product at $T \rightarrow \infty$,

$$\gamma^{\text{ht}} = \bar{\gamma}_{(T \rightarrow \infty)} = \left(\frac{1}{3n-3}\right) \sum_{i=4}^{3n} \gamma_i \quad (7)$$

and q^{ht} is given by

$$q^{\text{ht}} = \frac{\partial \ln \gamma^{\text{ht}}}{\partial \ln V} \quad (8)$$

For forsterite, we get $q^{\text{ht}} = 1.257$, $K' = 4.001$, and an isobaric temperature derivative of bulk modulus ($\partial K_T / \partial T$), of -174.592 bar/K (i.e., ≈ -0.017 GPa/K). The procedure disregards the fact that, at low T , the bulk modulus would

presumably vary nonlinearly with temperature. However, as we see in Fig. 6, this nonlinearity is virtually absent in the experimental data for the alpha polymorph. The calculated thermal effect on K is lower than that obtained by the best fit to the experimental data, but lies within the uncertainty range obtained by Meng et al. (1993) (i.e. $\left(\frac{\partial K}{\partial T}\right) = -0.0214 \pm 0.03$ GPa/K) from a least squares fit of the measured thermal pressure. Moreover, by coupling the αK product with the isobaric temperature derivative, we obtain the ab initio thermal expansion that is in good agreement with the experimental data of Matsui and Manghnani (1985) (Fig. 7).

The computed α values may be recast into a T -polynomial with negligible error in reproducibility (Table 4). The change of sign in the second derivative of the $\alpha_T(T)$ at high T is very likely an artefact of the approximations introduced in the quasi-harmonic gamma-mode analysis of frequencies. The non-zero α_0 coefficient in the α_T versus T polynomial for forsterite solves the purpose of maintaining a constant slope in the $\alpha = f(T)$ relation at high T .

For the calculation of thermodynamic properties, we combine the Kieffer's model (Kieffer 1979a, b) for acoustic modes and the Einstein model for optic modes. In the harmonic approximation, the isochoric heat capacity, C_V , of one mole of a solid is then given by the relation

$$C_V = \frac{3R}{Z} \left(\frac{2}{\pi}\right)^3 \sum_{i=1}^3 \int_0^{X_i} \frac{[\arcsin(X/X_i)]^2 X^2 e^X dX}{(X_i^2 - X^2)^{1/2} (e^X - 1)^2} + \frac{R}{Z} \sum_4^{3n} e^{X_i} \left(\frac{X_i}{e^{X_i} - 1}\right)^2 \quad (9)$$

where n is the number of atoms and Z is the number of formula units per unit cell. The first term on the right is the acoustic contribution at \mathbf{k}_{max} , which is represented in terms of a sine-wave dispersion relation [Kieffer 1979a, b; Table S2 (supplementary material)]. The second term is the contribution of all remaining (optic) modes. The C_V of forsterite, computed according to Eq. 9 attains the Dulong–Petit limit at high temperature. The C_V values have been calculated using ab initio vibrational frequencies, and also using a scaling factor to these frequencies that is discussed

Table 4 Quasi-harmonic analysis of vibrational modes, and the derived thermodynamic parameters

| Phase | q^{ht} | $(\alpha K)_\infty$ Bar/K | $(dK/dT)_P$ Bar/K | $\alpha_0 \times 10^7$ – | $\alpha_1 \times 10^7$ K ⁻¹ | $\alpha_2 \times 10^3$ K ⁻² | α_3 K ⁻³ | α_4 K ⁻⁴ |
|--|-----------------|------------------------------|----------------------|-----------------------------|---|---|-------------------------------|-------------------------------|
| α -Mg ₂ SiO ₄ | 1.257 | 46.632 | -174.592 | 0.10031 | 269.31 | 5.6082 | -2.6162 | 243.828 |
| β -Mg ₂ SiO ₄ | 3.262 | 54.831 | -117.997 | 0.00000 | 464.00 | -13.8005 | 3.6196 | -395.094 |
| γ -Mg ₂ SiO ₄ | 3.283 | 51.053 | -104.108 | 0.00000 | 323.00 | -7.3084 | 1.3745 | -150.406 |

$(\alpha K)_\infty$ and $(dK/dT)_P$ are in bar/K. $\alpha_T = \alpha_0 T + \alpha_1 + \alpha_2 T^{-1} + \alpha_3 T^{-2} + \alpha_4 T^{-3}$. Thermal expansion expression valid in the T range $200 \leq T$ (K) $\leq 3,000$

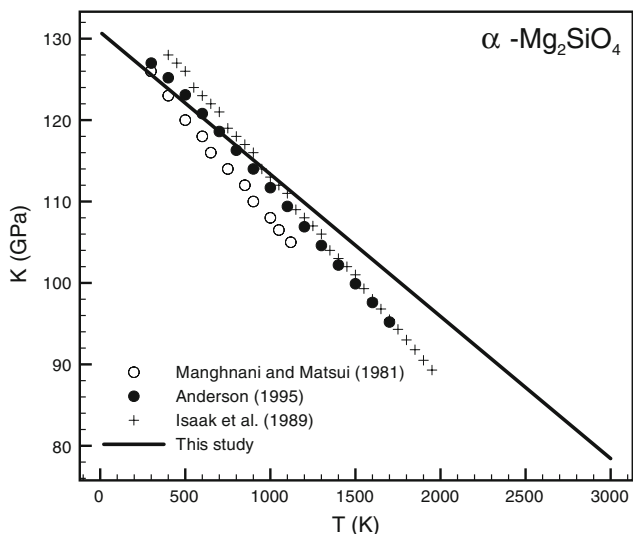


Fig. 6 Computed isobaric thermal derivative of the bulk modulus of forsterite, compared with experiments (Manghnani and Matsui 1981; Isaak et al. 1989) and literature estimates (Anderson 1995)

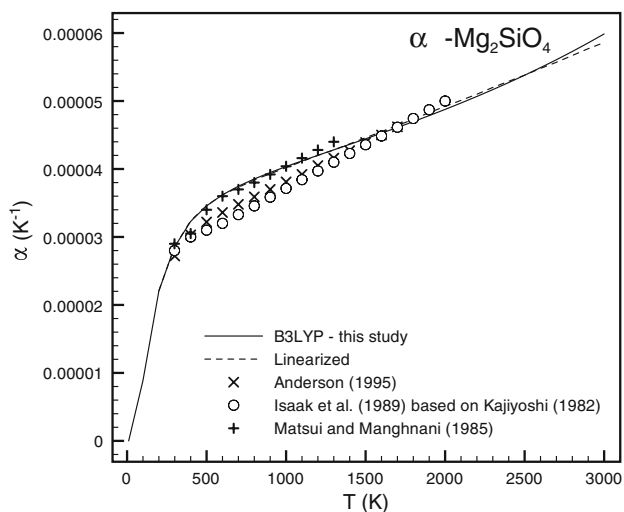


Fig. 7 Isobaric thermal expansion of forsterite, compared with experiments and estimates. The *dashed line* is the linearized function of $\alpha_T = f(T)$

later. The isobaric heat capacity, C_P , can be computed from C_V using the standard relation

$$C_P = C_V + T\alpha_T^2 K_{P,T} V_{P,T} \quad (10)$$

Figure 8 illustrates the calculated C_P versus T relation, using scaled vibrational frequencies to compute C_V (the scaling of vibrational frequencies is discussed later). At 298 K, the calculated C_P with unscaled vibrational frequencies, is 116.8 J/[mol \times K], which is quite close to the calorimetric value of 117.9 J/[mol \times K], (Robie et al. 1982) but significantly lower than the value 119.3 J/[mol \times K] that was computed at LDA level of theory by Li et al. (2007).

In the high- T range, where optical contributions to thermal properties are dominant, the computed C_P is in agreement with the calorimetric data tabulated in Robie et al. (1978).

The semiclassical C_P versus T data of forsterite between 298.15 and 3,000 K have been fitted by the Haas–Fisher polynomial expression of C_P as a function of T (Haas and Fisher 1976)

$$C_P = a + b \times T + c \times T^{-2} + d \times T^2 + e \times T^{-1/2} \quad (11)$$

The regression coefficients, are listed in Table 5. The Haas–Fisher polynomial reproduces the computed semiclassical C_P data with a mean error of 0.2 J/[mol \times K], the summation of χ^2 residuals over 28 values being 4.80×10^{-5} .

In the absence of configurational disorder, the entropy of one mole of crystalline substance can be expressed as

$$\begin{aligned} S &= S_{\text{trans}} + S_{\text{vib}} + S_{\text{el}} + S_{\text{an}} \\ &= \frac{3R}{Z} \left(\frac{2}{\pi}\right)^3 \sum_{i=1}^3 \int_0^{X_i} \frac{[\arcsin(X/X_i)^2] X dX}{(X_i^2 - X^2)^{1/2} (e^X - 1)} \\ &\quad - \frac{3R}{Z} \left(\frac{2}{\pi}\right)^3 \sum_{i=1}^3 \int_0^{X_i} \frac{[\arcsin(X/X_i)^2]}{(X_i^2 - X^2)^{1/2}} \ln(1 - e^{-X}) dX \\ &\quad + \frac{R}{Z} \sum_{i=4}^{3n} \left(\frac{X_i}{e^{X_i} - 1} - \ln(1 - e^{-X_i}) \right) \\ &\quad + \frac{R}{Z} \ln(Q_e) + \int_0^T V_T K_T \alpha_T^2 \end{aligned} \quad (12)$$

The first two terms on the right after the second equality of this equation represents the sine-wave dispersion contributions (acoustic modes) according to the Kieffer model (Kieffer 1979a, b). The third term is the optical contribution of the remaining $3n-3$ (optic) modes. The fourth term is the electronic contribution arising from spin multiplicity (here identically equal to zero for all the investigated phases) and the last term is the anharmonic contribution to the entropy of the substance.

The commonly accepted value of entropy for forsterite at 1 bar, 298 K is 94.11 J/[mol \times K] (Berman 1987; Holland and Powell 1990; Saxena et al. 1993). We obtain a somewhat lower value of 92.5 J/[mol \times K] from the semiclassical calculations. However, this disagreement essentially disappears when a scaling factor is applied to the ab initio vibrational frequencies as will be discussed later on, and mentioned above in the section dealing with the calculation of C_V . (With the use of the same scaling factor the ab initio entropies of the β and γ phases are also

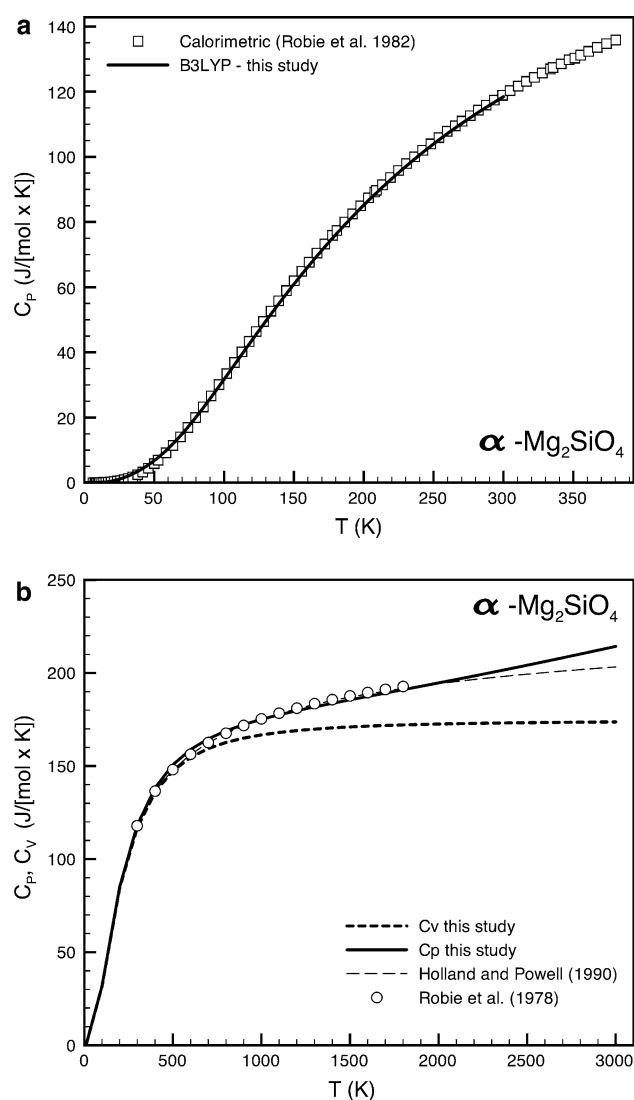


Fig. 8 **a** Semiclassically predicted low- T isobaric heat capacities of forsterite (scaled frequencies) compared with experiments. **b** Semiclassically predicted high- T isobaric heat capacities of forsterite compared with tabulated values. The isochoric heat capacity curve (dashed line) is also shown to attain, as it should, the $3nR$ Dulong–Petit limit at high temperature (n is the number of atoms per formula unit)

found to be in good agreement with their respective calorimetric third law entropies, as discussed below).

In the harmonic approximation the internal energy of the solid is given by:

$$U = E_{\text{ai,crystal}} + \frac{3RT}{Z} \left(\frac{2}{\pi}\right)^3 \sum_{i=1}^3 \int_0^{X_i} \frac{[\arcsin(X/X_i)]^2 X dX}{(X_i^2 - X^2)^{1/2} (e^X - 1)} + \frac{RT}{Z} \sum_{i=4}^{3n} X_i \left(\frac{1}{2} + \frac{1}{e^{-X_i} - 1}\right) \quad (13)$$

where the second and third terms on the right constitute the thermal correction to U , which we denote as Therm- U , and includes the zero-point energy. Adding the PV product to Therm- U , one obtains the thermal correction to enthalpy (Therm- H), and subtracting the TS product from Therm- H at the same P - T , one has the thermal correction to the Gibbs free energy (Therm- G). All thermal corrected parameters (Therm- U , Therm- H and Therm- G) are listed in Table S3 (supplementary material). Adding thermal corrections to B3LYP total energies ($E_{\text{B3LYP,crystal}}$) and summing up algebraically the various terms in a chemically balanced reaction, one obtains directly enthalpy and Gibbs free energy changes of the reaction at 1 bar, 298.15 without the need of assessing enthalpy and Gibbs free energy of formation from the elements, which are subject to considerable uncertainties, due to the difficulties in estimating the appropriate electronic energy for isolated gaseous atoms (see Ottonello et al. 2007; for a more detailed account of the problem).

Wadsleyite: (β -Mg₂SiO₄)

There are 28 atoms in the orthorhombic bipyramidal unit cell of the beta polymorph of Mg₂SiO₄. The irreducible representation of vibrational modes, with a group theoretical treatment of the optical zone-center (Γ point; $\mathbf{k} = 0$) yields

$$\Gamma = 12B_{2g} + 10B_{2u} + 9B_{3g} + 12B_{3u} + 7A_u + 7B_{1g} + 13B_{1u} + 11A_g \quad (14)$$

In Table S4 (supplementary material) we list the vibrational frequencies obtained in this study and their mode-gamma analysis.

The B3LYP computed data are in agreement with the results of recent theoretical calculations by Wu and Wentzcovitch (2007) at the LDA level of theory and experimental data from infrared and Raman measurements (see Wu and Wentzcovitch 2007; and reference therein).

Table 5 Ab initio volume (J/bar), entropy (J/[mol × K]) and Haas–Fisher isobaric (1 bar) heat capacity coefficients for the investigated phases

| Phase | $V_{298.15}^\circ$ | $S_{298.15}^\circ$ | $a \times 10^{-2}$ | $b \times 10^2$ | $c \times 10^{-6}$ | $d \times 10^5$ | $e \times 10^{-2}$ |
|--|--------------------|--------------------|--------------------|-----------------|--------------------|---------------------|---------------------|
| α -Mg ₂ SiO ₄ | 4.4794 | 92.452 (94.114) | 1.5555 (1.5513) | 2.1449 (2.1307) | -4.4249 (-4.4060) | -0.08423 (-0.07918) | 0.63793 (0.87536) |
| β -Mg ₂ SiO ₄ | 4.1530 | 85.662 (87.316) | 1.5854 (1.6139) | 2.3753 (2.2270) | -4.2454 (-4.1112) | -0.27587 (-0.24731) | -0.39472 (-0.86514) |
| γ -Mg ₂ SiO ₄ | 4.0026 | 80.183 (81.715) | 1.5363 (1.5346) | 2.1642 (2.1405) | -4.7897 (-4.7490) | -0.31483 (-0.30796) | 1.0957 (1.2708) |

Values in parentheses obtained with scaled frequencies (see text for details)

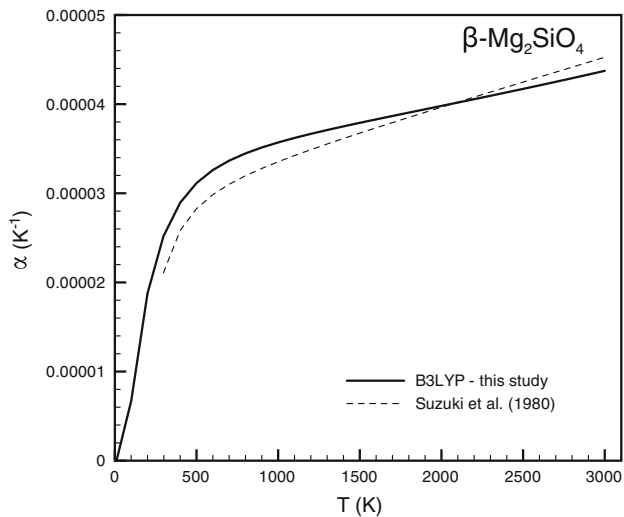


Fig. 9 Comparison of the Isobaric thermal expansion coefficient versus T of wadsleyite, as calculated in this study, with the experimental data of Suzuki et al. (1980)

According to the experimental data of Meng et al. (1993), the αK product of wadsleyite increases from 3.65×10^{-3} GPa/K at 300 K to a constant value of 5.16×10^{-3} GPa/K above its Debye temperature. Our gamma mode analysis of ab initio frequencies yields an average value of αK of 5.48×10^{-3} GPa/K at high temperature. As illustrated in Fig. S8 (supplementary material), our results agree with Meng et al. (1993) within the experimental uncertainty of the data.

Proceeding in the same manner as done for forsterite, we obtained the isobaric temperature derivative of the bulk modulus of wadsleyite to be -0.012 GPa/K, which is substantially smaller in magnitude than the experimental data of Fei et al. (1992) on β -($\text{Mg}_{0.84}\text{Fe}_{0.16}$) $_2\text{SiO}_4$ (-0.027 GPa/K). However, our results for thermal expansion are roughly consistent with the data of Suzuki et al. (1980) (Fig. 9; Table 4).

The low-temperature semiclassical C_p values are in good agreement with the recent calorimetric measurements of Akaogi et al. (2007) (Fig. 10a). The computed high-temperature C_p values are also in good agreement with the thermodynamic assessment of Jacobs and de Jong (2005) up to 1,500 K (Fig. 10b). For higher temperature, our computation gives values intermediate between those of Jacobs and de Jong (2005) and Watanabe (1982) (refitted by Fei and Saxena 1986).

The Haas–Fisher polynomial expansion (Table 5) reproduces computed heat capacities with a mean error of 0.6 J/[mol \times K]. The summation of χ^2 -residuals over 28 values is 4.63×10^{-4} . The B3LYP predicted entropy at 1 bar, 298.15 K is 85.7 J/[mol \times K], which is close to the value of 86.4 ± 0.4 J/[mol \times K] determined recently by

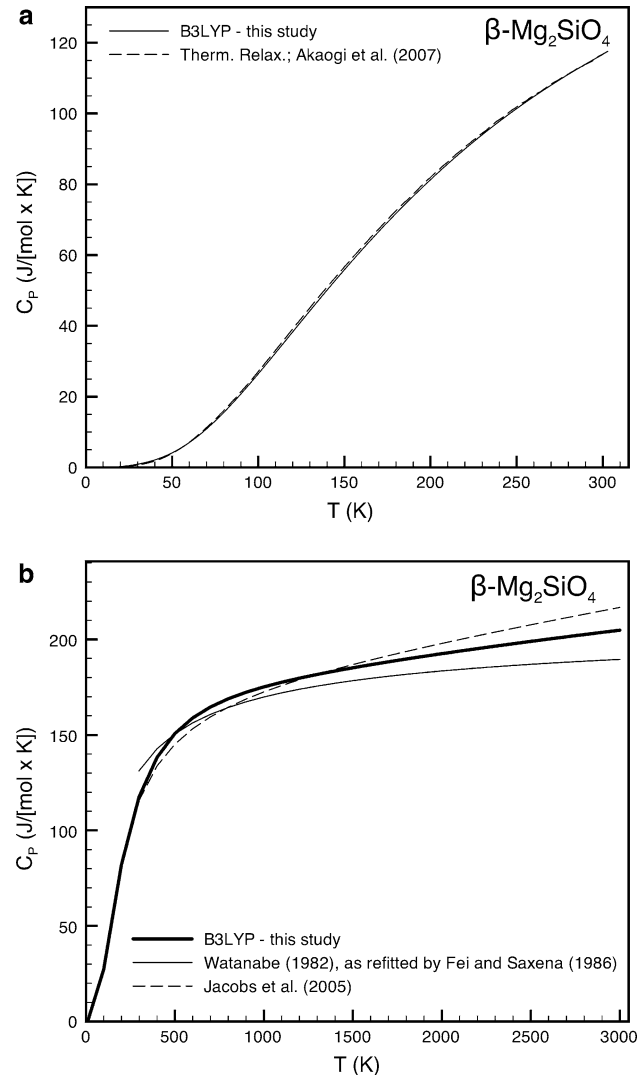


Fig. 10 **a** Semiclassically predicted low- T isobaric heat capacities of wadsleyite compared with the results of recent calorimetric experiments. **b** Comparison of high- T isobaric heat capacity of wadsleyite calculated in this study (semiclassical) with that of Jacobs and de Jong (2005) and Watanabe (1982), as refitted by Fei and Saxena (1986)

Akaogi et al. (2007) using their low-temperature calorimetric data, and somewhat lower than the 88.7 J/[mol \times K] predicted by Wu and Wentzcovitch (2007). The third law entropy values determined in this study and by Akaogi et al. (2007) are significantly lower than those of Jacobs and de Jong (2005) (91.3 J/[mol \times K]) and Saxena et al. (1993) (93.0 J/[mol \times K]).

Ringwoodite (γ - Mg_2SiO_4)

There are 14 atoms in the Cubic Hexakisoctahedral unit cell corresponding to 39 true vibrational modes. The irreducible representation of vibrational modes, with a group

theoretical treatment of the optical zone-center (Γ point; $\mathbf{k} = 0$) yields

$$\Gamma = 6E_u + 1B_u + 2E_g + 1A_g + 3F_{1g} + 9F_{2g} + 12F_{1u} + 6F_{2u} \quad (15)$$

In Table S5 (supplementary material) we list the vibrational frequencies obtained in this study and their mode- Γ analysis. The results compare well with the recent prediction by Yu and Wentzcovitch (2006) at the LDA level of theory and available experimental data (Chopelas et al. 1994).

The mode- Γ analysis of ab initio frequencies yields an average value of αK of 5.01×10^{-3} GPa/K at high temperature, which is somewhat larger than the αK value of 4.54×10^{-3} GPa/K above the Debye temperature that was determined by Meng et al. (1993) on the basis of in situ high P - T - X diffraction studies. Our ab initio αK values are, however, much larger than the estimates of Saxena et al. (1993) at all temperature above ~ 500 K [Fig. S9 (supplementary material)].

Using the limiting value of the αK product for $T \rightarrow \infty$ (51.052 bar/K) the ab initio bulk modulus at the athermal limit (196.389 GPa) and its isothermal pressure derivative ($K' = 4.322$) we deduce a value of -0.010 GPa/K for the isobaric thermal derivative of the bulk modulus of ringwoodite, which is much lower than the value of -0.028 ± 3 given by Meng et al. (1993). However, as illustrated in Fig. 11, our results for the thermal expansion coefficient as a function of temperature agree very well with the experimental data of Suzuki et al. (1979) and Ming et al. (1992) (Fig. 11; Table 4).

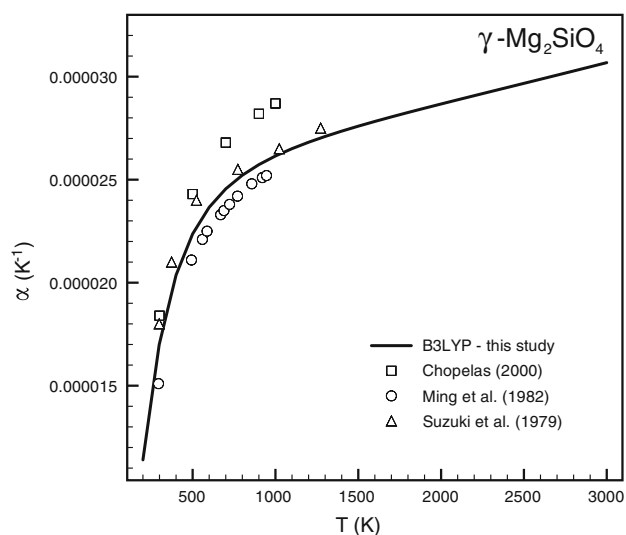


Fig. 11 Computed thermal expansion of ringwoodite compared with the experimental data of various authors. The *bold line* is the thermal expansion derived from ab initio calculations

We determined the isochoric and isobaric heat capacities of ringwoodite following the same procedure as used in the derivation of these thermochemical properties for the other polymorphs, as discussed above. The computed low-temperature C_p values are again in good agreement with the recent calorimetric data of Akaogi et al. (2007) (Fig. 12a), while the high- T values are in good agreement with those of Chopelas et al. (1994), and Watanabe (1982) (Fig. 12b) Haas–Fisher coefficients of polynomial fitting of high- T semiclassical isobaric heat capacity are listed in Table 4. The polynomial function reproduces computed

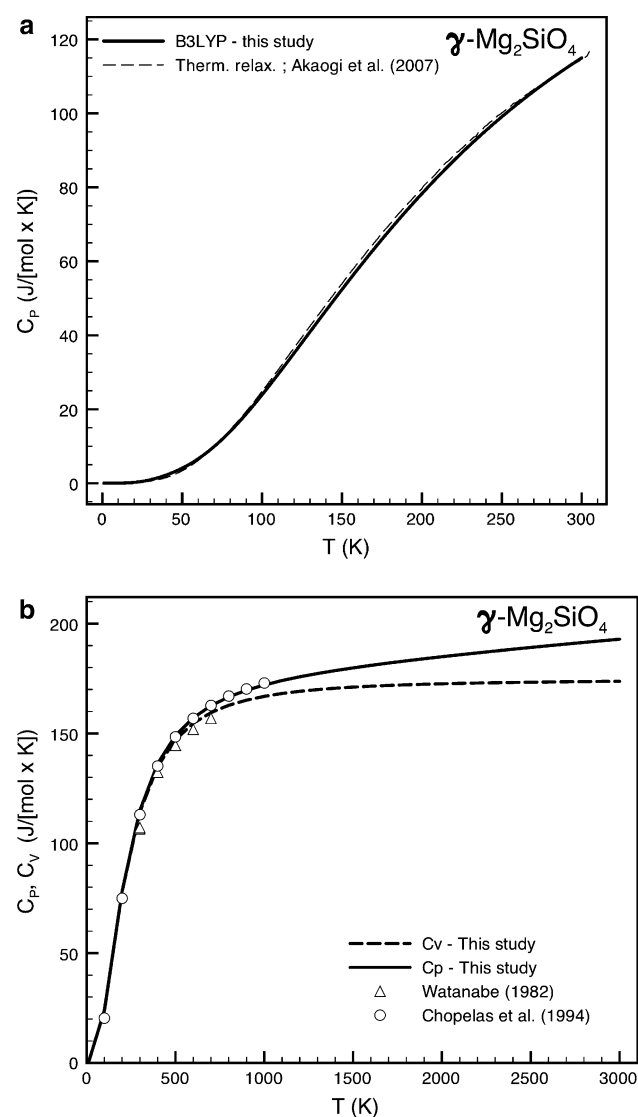


Fig. 12 **a** Semiclassically predicted low- T isobaric heat capacities of ringwoodite compared with the results of recent calorimetric experiments. **b** Semiclassically predicted isochoric and isobaric heat capacities of ringwoodite. The isobaric heat capacity data of Chopelas et al. (1994) and Watanabe (1982) are superimposed for comparative purposes

heat capacities with a mean error of 0.6 J/[mol × K]). The summation of χ^2 residuals over 28 values is 5.71×10^{-5} .

Our semiclassically computed third law entropy at 1 bar, 298 K is 80.2 J/[mol × K]), which is close to the recent third law value of 82.7 ± 0.5 J/mol-K determined by Akaogi et al. (2007) from calorimetric C_P data, but is significantly lower than the estimates of Fei et al. (1990) (89.0 J/[mol × K]), Jacobs and de Jong (2005) (88.1–91.8 J/[mol × K]), depending on the adopted volume estimates) and Yu and Wentzcovitch (2006) (85 J/[mol × K]).

Discussion: ab initio and semiclassical calculations, volume refinement and scaling of vibrational frequencies

Within the lattice dynamics theory, the calculation of thermodynamic properties requires the knowledge of the full phonon dispersion relation and the corresponding vibrational density of states (VDOS). Thermodynamic functions are then expressed as averages over the VDOS. Because of this averaging, thermodynamic properties are insensitive to details of the VDOS and even simplified models can be adopted such as the Kieffer's model 1979a, b that was successfully applied to solids and also recently by Jacobs and De Jong (2003) and Jacobs et al. (2006). As already discussed, the Kieffer's model approximates the VDOS for acoustic modes through a sine-like dispersion relation related to group velocities in combination with an Einstein's model for optic modes. As a demonstration of the validity of such an approach, in Table 6 we report a comparison of computed isobaric heat capacity and entropy at

Table 6 Comparison of computed isobaric heat capacity and entropy at 298 K for Mg_2SiO_4 polymorphs with both ab initio results obtained at the LDA level by means of a full calculation of the VDOS and recent experimental data from calorimetric measurements

| | Present study ^a | | LDA (full VDOS) ^b | Exp. ^c |
|------------------------|----------------------------|--------|------------------------------|-------------------|
| | Unscaled | Scaled | | |
| C_P (J/[mole × K]) | | | | |
| α - Mg_2SiO_4 | 116.8 | 117.9 | 119.3 | 117.9 |
| β - Mg_2SiO_4 | 116.2 | 117.3 | 118.1 | 116.3 |
| γ - Mg_2SiO_4 | 113.2 | 114.5 | 116.9 | 114.0 |
| S (J/[mole × K]) | | | | |
| α - Mg_2SiO_4 | 92.5 | 94.1 | 95.9 | 94.1 |
| β - Mg_2SiO_4 | 85.7 | 87.3 | 88.7 | 86.4 |
| γ - Mg_2SiO_4 | 80.2 | 81.7 | 85.0 | 82.7 |

^a See text for further details

^b Li et al. 2007; Wu and Wentzcovitch 2007; Yu and Wentzcovitch 2006

^c Akaogi et al. (2007)

298 K for Mg_2SiO_4 polymorphs with both ab initio results obtained at the LDA level by means of a full calculation of the VDOS (Li et al. 2007; Wu and Wentzcovitch 2007; Yu and Wentzcovitch 2006) and recent experimental data from calorimetric measurements (Akaogi et al. 2007). Here, the computed B3LYP vibrational frequencies were used for the optic modes. Although the adopted semiclassical model lacks of the rigor of a complete lattice dynamics, it surprisingly gives very good results.

A further comment is needed concerning the contribution of LO and TO modes at Γ -point on thermodynamic properties. With respect to previous discussion on VDOS, we expect that the LO–TO splitting hardly affect thermodynamic functions. To prove that, we used data reported in Table S2 (supplementary material) for forsterite and we simply averaged LO–TO frequencies. An increase of 0.8 J/(mol × K) in the optical contribution to the bulk entropy and heat capacity is observed, with respect to the Γ point analysis while thermal corrections to U and H decrease of 0.5 kJ/mol. Although this procedure is rather crude to be proposed as a predictive tool it indicates that the correction is rather small. Therefore, in the present work the thermodynamic analysis was based on computed TO frequencies.

In estimating the molar volume at 1 bar, 298.15 K, we started from the static volume at the athermal limit, neglecting the contribution of vibrational pressure which arises from thermal energy at zero point. This vibrational contribution to the zero point volume can be assessed through application of the approximate Born–Huang relation (Born and Huang 1954).

$$\frac{V_0 - V_{0,st}}{V_{0,st}} = \frac{9}{8} \times \frac{\gamma n R \Theta_D}{V_0 K_0} \quad (16)$$

where Θ_D is the elastic or “characteristic” Debye temperature obtained from acoustic frequencies and the other symbols have their usual meaning.

From the data summarized in Table 7, we find that the contribution of the zero-point vibrational terms to the zero point volume is non-negligible. In the case of wadsleyite, the increase of 0.040 J/bar computed by us is in good agreement with the previous estimates of Jacobs et al. (2006) (i.e. 0.045 J/bar). Unfortunately, the predicted volume shifts further worsen the disagreement between the semiclassical B3LYP predictions and the experimental

Table 7 Contribution of acoustic branches to the zero point volume of the investigated substances

| Phase | Θ_D | E_{ac}° (hartree) | V° (J/bar) | ΔV (J/bar) |
|------------------------|------------|--------------------------|-------------------|--------------------|
| α - Mg_2SiO_4 | 750 | 0.00028566 | 4.5154 | 0.0472 |
| β - Mg_2SiO_4 | 896 | 0.00034127 | 4.1837 | 0.0402 |
| γ - Mg_2SiO_4 | 880 | 0.00033517 | 4.0168 | 0.0201 |

Elastic Debye temperatures and thermal energies are also listed

data. This problem, and the fact that Eq. 16 was obtained by factoring out the discrete mode-gammas of the individual acoustic branches, which is only a crude approximation of a more complex reality (the electronic energy arising from the acoustic modes is roughly 1% of the bulk zero point energy of the substance; cf. Tables S3 and 7), lead us to disregard the vibrational contribution to the zero-point volume.

We now consider the sensitivity of vibrational properties to the equilibrium lattice parameters. The expected range of uncertainty in the determination of V_0 with the CRYSTAL default computational procedure is smaller than 1% (Pascale et al. 2004). We first observe that cell volume variations of 6% in either direction, which correspond to an energy change of 0.003 hartree, induce a maximum shift of about 100 cm^{-1} in the wave number. The variation of the vibrational frequencies with volume is quite regular, as shown in Fig. 13, for the 11 A_g modes of forsterite. The largest excursion in the 0.94–1.06 V_0 range for A_g modes is 96 cm^{-1} . An 1% change on the calculated volume at the athermal limit corresponds roughly to a maximum uncertainty of 16 cm^{-1} on the adopted wavenumber.

As one would see in Fig. 13, the curvature of the frequency shift is almost negligible in the investigated range. In evaluating the thermal effect on the isobaric compressibility of the investigated phases, we factored out the mode-gammas of the individual modes (Eqs. 8–10) implicitly assuming them to be independent on temperature. More complex analyses may be eventually carried out. Jacobs et al. (2006), for example, proposed a Taylor expansion of logarithmic terms truncated to the third degree:

$$\ln\left(\frac{v_i(V)}{v_i(V_0)}\right) = -\gamma_{i,0} \ln\left(\frac{V}{V_0}\right) - \frac{1}{2} q_{1,i,0} \gamma_{i,0} \ln^2\left(\frac{V}{V_0}\right) - \frac{1}{6} q_{2,i,0} \gamma_{i,0} (q_{1,i,0} + q_{2,i,0}) \ln^3\left(\frac{V}{V_0}\right) \quad (17)$$

where

$$\gamma_{i,0} = \left(\frac{\partial \ln v_i}{\partial \ln V}\right)_{T=0, P=0}; \quad q_{1,i,0} = \left(\frac{\partial \ln \gamma_i}{\partial \ln V}\right)_{T=0, P=0}; \\ q_{2,i,0} = \left(\frac{\partial \ln q_i}{\partial \ln V}\right)_{T=0, P=0}$$

Writing the vibrational frequency as dependent upon an anharmonicity parameter a for each mode of vibration i , one has a more precise way of depicting the frequencies in the T – V space:

$$v(T, V) = v(V)(1 + aT) \quad (18)$$

According to Jacobs et al. (2006) the anharmonicity parameter is always negative and assumes, in the case of forsterite, values of the order 10^{-5} K^{-1} .

T -dependent mode-gammas could be of some utility only in the high- T region where the quasi-harmonic analysis fails due to anharmonic effect that is highlighted by the direct comparison of computed and experimental thermal pressures (see, for example, Fig. 10.1 in Anderson 1995). We have already seen that such anharmonic effect could be relevant for the high- P polymorph ringwoodite at $T > 2,000 \text{ K}$ [Fig. S9 (supplementary material)], but we have no clear idea as yet on the importance of this effect for the other two polymorphs.

The accurate ab initio all electron investigation at the B3LYP level reported by Noel et al. (2006) of the vibrational behavior of the α -polymorph makes it possible to precisely assign all experimental measurements to discrete IR and Raman active modes of the mineral (see their Tables 5, 7). Although the LO/TO splitting, not taken into account in the present work, prevents a detailed analysis of computed frequencies of the IR-active data, the comparison between the experimental Raman-active wave numbers (Servoin and Piriou 1973; Iishi 1978; Hofmeister 1987; Chopelas 1991; Reyand 1991; Kolesov and Geiger 2004) and the computed frequencies shows a good agreement ($R^2 = 0.993$ – 0.995), and indicates scaling factors in the range 0.985–0.989 (slope coefficients) between experimental and computed data (Fig. 14).

The need for a scaling factor between ab initio harmonic frequencies and experimental observation is widely recognized (e.g. Scott and Radom 1996). Application of the scaling factor to the ab initio vibrationally dependent thermodynamic parameters yields discrete values that are more consistent with the experimental results and/or classical thermodynamic deductions (values in brackets in Table 5). When the same basis set and theoretical

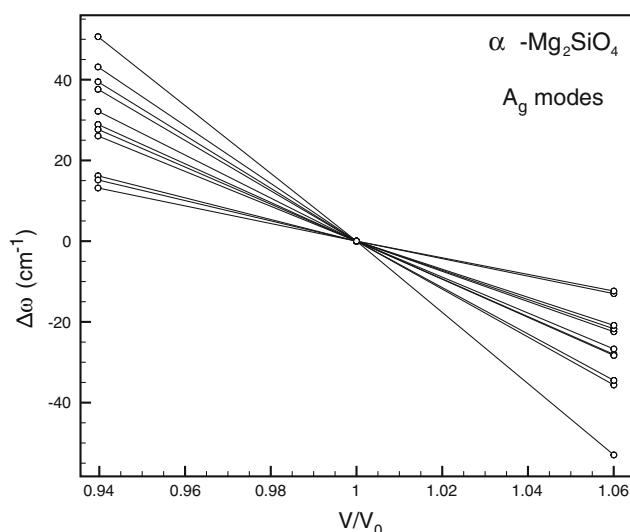


Fig. 13 Dependence of vibrational frequencies of forsterite on the cell volume V . Eleven vibrational mode frequencies of A_g symmetry are represented with their quadratic fitting curves. Frequencies are referred to the respective values at the equilibrium cell volume V_0

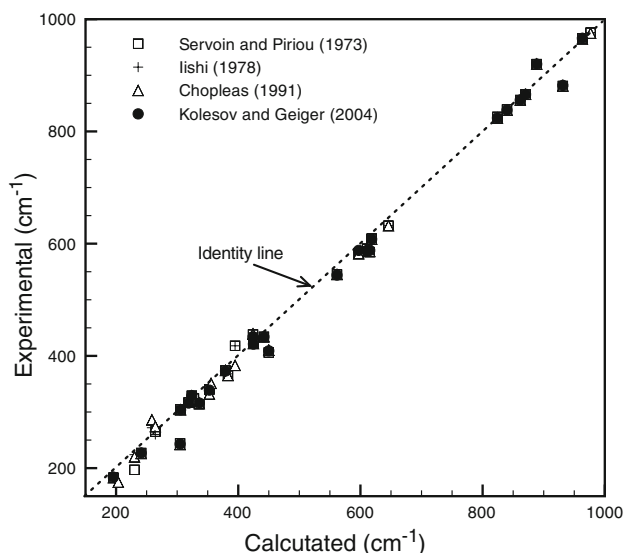


Fig. 14 Calculated versus experimental Raman-active wave numbers of forsterite. Slope coefficients between ab initio and experimental sets range from $y = 0.985x$ to $y = 0.989x$, not far from the identity condition $y = x$

treatment are applied to all phases, the scaling procedure has a negligible effect on the relative stabilities of the various polymorphs. However, in general, the values computed for heat capacity and entropy of the individual Mg_2SiO_4 polymorphs, which are summarized in the Table 8, are found to be in good agreement with the experimental data when the ab initio harmonic frequencies are subjected to the mean scaling factor of 0.9875.

This is illustrated by a comparison between ab initio and experimental data for the Raman active wave numbers for forsterite (Fig. 14). For α -polymorph, the semiclassical C_p (117.9 J/[mol \times K]) and S^0 (94.11 J/[mol \times K]) values at 298 K, calculated on the basis of scaled frequencies, are effectively the same as the corresponding calorimetric values (identical to the first and second decimal places, respectively) tabulated by Robie et al. (1982). For the β -polymorph, we get, using scaled frequencies, $S^0(1 \text{ bar}, 298 \text{ K}) = 87.3 \text{ J/[mol} \times \text{K]}$, which is close to the recent calorimetric datum of $86.4 \pm 0.4 \text{ J/[mol} \times \text{K]}$ of Akaogi et al. (2007). For the γ -polymorph, the scaling factor based semiclassical $S^0(1 \text{ bar}, 298 \text{ K}) = 81.7 \text{ J/[mol} \times \text{K]}$, which is again in close agreement with the recent third law calorimetric value of $82.7 \pm 0.5 \text{ J/[mol} \times \text{K]}$ determined by Akaogi et al. (2007).

Application to phase equilibria

The first obvious application of our investigation is the appraisal of the univariant equilibria governing the relative stabilities of forsterite (α), wadsleyite (β) and ringwoodite (γ) in the P - T space. The relevant reactions are:

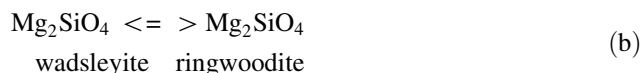
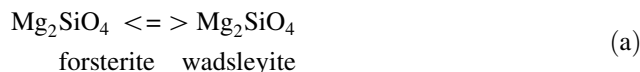


Table 8 Recommended predicted thermo-chemical properties of Mg_2SiO_4 polymorphs at 1 bar, 298 K

| Magnitude | | Forsterite (alpha) | Wadsleyite (beta) | Ringwoodite (gamma) |
|--------------------------------------|--------------------|--------------------|-------------------|---------------------|
| V° (J/bar) | | 4.437 | 4.087 | 3.963 |
| S° (J/[mol \times K]) | | 94.1 | 87.3 | 81.7 |
| C_p (J/[mol \times K]) | $a \times 10^{-2}$ | 1.5513 | 1.6139 | 1.5346 |
| | $b \times 10^2$ | 2.1307 | 2.2270 | 2.1405 |
| | $c \times 10^{-6}$ | -4.4060 | -4.1112 | -4.7490 |
| | $d \times 10^5$ | -0.0792 | -0.2473 | -0.3080 |
| | $e \times 10^{-2}$ | 0.87536 | -0.86514 | 1.2708 |
| Thermal expansion (K ⁻¹) | α_0 | 0.10031 | 0 | 0 |
| | α_1 | 269.31 | 464.00 | 323.00 |
| | α_2 | 5.6082 | -13.8005 | -7.3084 |
| | α_3 | -2.6162 | 3.6196 | 1.3745 |
| | α_4 | 243.828 | -395.094 | -150.406 |
| K_0 (GPa) | | 130.8 | 161.8 | 196.4 |
| K' | | 4.001 | 4.415 | 4.322 |
| $(dK/dT)_P$ (bar/K) | | -174.592 | -117.997 | -104.108 |
| Reaction (kJ/mol) | ΔH | ΔG | | |
| Alpha \rightleftharpoons beta | 33.592 | 35.619 | | |
| Beta \rightleftharpoons gamma | 12.429 | 14.099 | | |

Table 9 Changes of thermodynamic properties for polymorphic transitions of Mg₂SiO₄

| Parameter | α/β Transition | β/γ Transition | Notes |
|----------------------------------|---------------------------|---------------------------|--|
| ΔV (J/bar) | -0.326 | -0.150 | <i>This work</i> |
| | -0.350 | -0.1235 | <i>This work; ΔV optimized</i> |
| | -0.316 | -0.102 | Akaogi et al. (2007) |
| | -0.313 | -0.089 | Saxena et al. (1993) |
| | -0.332 | -0.080 | Jacobs et al. (2006) |
| ΔS (J/[mole \times K]) | -6.790 | -5.479 | <i>This work</i> |
| | -6.798 | -5.601 | <i>This work; scaled ω</i> |
| | -7.7 \pm 0.4 | -3.7 \pm 0.6 | Akaogi et al. (2007) |
| | -1.110 | -4.000 | Saxena et al. (1993) |
| | -1.040 | -4.800 | Jacobs et al. (2006) |
| ΔH (kJ/mole) | 33.649 | 12.442 | <i>This work</i> |
| | 33.592 | 12.429 | <i>This work; scaled ω</i> |
| | 27.2 \pm 3.6 | 12.9 \pm 3.3 | Akaogi et al. (2007) |
| | 32.1 | 8.8 | Saxena et al. (1993) |
| | (29.1) | (7.6) | Jacobs et al. (2006) |
| ΔG (kJ/mole) | 35.611 | 14.029 | <i>This work</i> |
| | 35.619 | 14.099 | <i>This work; scaled ω</i> |
| | 29.5 \pm 3.6 | 14.0 \pm 3.3 | Akaogi et al. (2007) |
| | 32.4 | 9.992 | Saxena et al. (1993) |
| | (29.4) | (9.03) | Jacobs et al. (2006) |
| Slope (MPa/K) | 2.080 | 3.643 | <i>This work</i> |
| | 1.965 | 4.401 | <i>This work; ΔV optimized</i> |
| | 1.968 | 4.499 | <i>This work; optimized ΔV and scaled ω</i> |
| | 2.436 | 3.627 | Akaogi et al. (2007) |
| | 3.55 | 4.494 | Saxena et al. (1993) |
| | 3.2 | 6 | Jacobs et al. (2006) |

Computed results are compared with other current estimates.

Values in brackets are retrieved by graphical interpolation of the data in the refereed work

The changes of Gibbs free energies (ΔG), enthalpies (ΔH), entropies (ΔS) and volumes (ΔV) of these reactions at the standard state (pure end-member phase at $T = 298.15$ K and $P = 1$ bar) are listed in Table 9. Gibbs free energy and enthalpy of reaction were readily obtained by summing up algebraically the electronic energies and the thermal corrections of the two polymorphs at equilibrium. The Clapeyron (P - T) slope of a reaction at any state is simply the ratio $\Delta S/\Delta V$ at that state.

The data summarized in Table 9 show that the computed enthalpy changes of the phase transitions are comparable to the experimental data and estimates found in the recent literature. In the case of β/γ transition the agreement with the high-temperature drop-solution calorimetric datum of Akaogi et al. (2007) is amazingly good, especially considering the fact that the transition enthalpy is ~ 4.8 ppm of the bulk energy of the two polymorphs at equilibrium. We also note from the data in Table 9 that the frequency scaling does not significantly affect the standard state Gibbs free energy and enthalpy changes for the β/γ transition, and its Clapeyron slope, which are in good

agreement with the estimates of Akaogi et al. (2007). For the the α/β transition our semiclassical standard state ΔG is close to the optimized value of Saxena et al. (1993), but the Clapeyron slope is more consistent with the data of Akaogi et al. (2007).

Comparison of the calculated equilibrium boundaries with the experimental data shows a discrepancy of ~ 2 GPa for the α/β (Fig. 15a) and ~ 4 GPa for the β/γ transitions (Fig. 15b).

The problem lies with the fact that, as already noted, the ab initio calculations somewhat overestimate the volumes of the phases. The failure of ab initio procedure to yield accurate volumetric data is a well known problem. Volumes for the calculation of α/β and β/γ transformations that are consistent with the semiclassical thermo-chemical and thermo-physical properties have been calculated by an optimization routine such that the net deviation of the calculated boundaries from the experimental data on phase transformation is minimized. For this purpose, we used the well known optimization program MINUIT (James and Roos 1977) and the experimental data from the following sources: Katsura and Ito (1989), Boehler and Chopelas

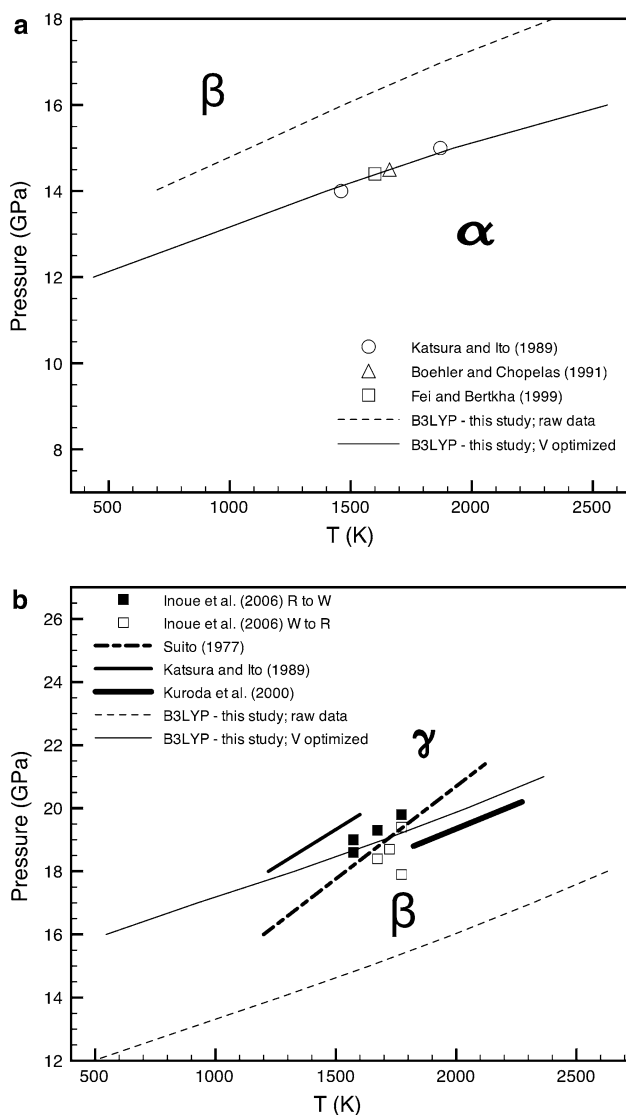


Fig. 15 **a** The univariant equilibrium between α and β polymorphs in the P - T space. Results of semiclassical calculations are compared with experimental data. Agreement with experiments is obtained by scaling the standard state volumes of the α and β polymorphs, respectively, to 4.4 and 4.05 J/bar. **b** The univariant equilibrium between β and γ polymorphs in the P - T space. Results of present calculations are compared with experimental observations. Agreement with experiments is obtained by scaling the standard state volumes of the β and γ polymorphs, respectively, to 4.05 and 3.925 J/bar

(1991), Fei and Bertkha (1999) for the α/β transition (equilibrium a) and the data of Inoue et al. (2006) for the β/γ transition (equilibrium b) and imposing all the relevant semiclassical thermodynamic parameters obtained in this study but volumes. Volumes were treated as independent variables bracketed by the ranges of uncertainty in experiments and estimates (Tables 1, 2, 3). A contouring procedure indicated that the problem was well behaved with centred minima and the absence of relative minima. The routine returned the following values $V_{\alpha} = 4.4372$ J/

bar; $V_{\beta} = 4.0869$ J/bar; $V_{\gamma} = 3.9634$ J/bar, which when applied in a direct way in conjunction with our semiclassical parameters generate the phase boundaries illustrated in Fig. 15. We may note that, while the optimised volume of ringwoodite is practically identical to the datum of Katsura and Ito (1989) (Table 3), the optimised volumes of forsterite and wadsleyite exceed the upper limits of experimental data (Tables 1, 2). The difference between the ab initio volumes and optimised ones is roughly constant and averages 5×10^{-2} J/bar, i.e. at the same level as the zero point contribution to static volumes.

We stress again that, although volume refinement is a necessary step, frequency scaling is unnecessary for the purpose of calculation of reliable univariant equilibria at high P conditions. Indeed, if we adopt the raw ab initio thermodynamic data (no scaling) and the optimized volumes, the Clapeyron boundaries are shifted upward of roughly +32 K for the $\beta \rightarrow \gamma$ transition and downward of -14 K for the $\alpha \rightarrow \beta$ and the slopes are virtually unaffected. Scaling of frequencies is, however, needed to obtain accurate entropy and heat capacity values of the individual phases.

Summary and conclusions

The thermophysical calculations carried out in this study using all-electron B3LYP energies show that the adoption of expanded basis sets, and appropriate sampling grids yield values of the vibrational thermodynamic properties of phases, namely C_P and S , and enthalpy and Gibbs free energy changes of reactions that could be sufficiently accurate for the purpose of subsolidus phase equilibrium calculations of minerals in the Earth's Mantle. Ab initio volumes are overestimated (by around 2.5%) and require readjustment on the basis of phase transition topology. Scaling of frequencies yields estimates of entropy and heat capacity of individual phases that are in very good agreement with experimental data (Robie et al. 1978; Akaogi et al. (2007), but is unnecessary in the calculation of phase boundaries. In the absence of reliable experimental data, the computational approach outlined in this study may be fruitfully adopted to fill the gap of knowledge concerning the topology of phase diagrams.

The thermo-chemical and thermo-physical properties of the Mg_2SiO_4 polymorphs and the ΔH and ΔG values of the polymorphic transitions at 1 bar, 298 K, as deduced in this study, are summarized in Table 8. Work is currently in progress to apply the present approach to calculate the thermodynamic properties of anhydrous phase B, stishovite and other mantle phases. Ultimately the thermo-chemical and thermo-physical data for mantle minerals would need to be optimized using selected high quality data from those

available in the literature on ab initio, or semiclassical, and calorimetric properties and phase equilibrium relations in order to develop an internally consistent data base that reproduce, within errors, well calibrated experimental reaction boundaries of the mantle minerals.

Acknowledgments We are indebted to Editor Masanori Matsui, and to two anonymous reviewers for their insightful advices and comments.

Appendix A

Basis set

The all-electron Gaussian-type basis set adopted is a 8–511G(d) for magnesium (Pascale et al. 2005), a 88–31G(d) set for silicon and a 8–411G(d) set for oxygen (Nada et al. 1996). Orbital exponents and contraction coefficients of each shell type are reported in Table S6 (supplementary material).

Effect of the grid for DFT numerical integration

The density functional theory (DFT) exchange–correlation contribution is evaluated by numerical integration over the cell volume (Pascale 2004). Radial and angular points of the atomic grid were generated through Gauss–Legendre and Lebedev quadrature schemes. Grid pruning has been applied, as discussed by Pascale et al. (2004), that contains M radial points and a variable number of angular points, with a maximum of N points on the Lebedev surface in the most accurate integration region. This is henceforth referred to as $(M, N)p$.

A preliminary investigation of the effect of the grid for DFT numerical integration on the static and vibrational features of γ - Mg_2SiO_4 , while keeping the structural parameters constant, indicate a negligible overall effect on the computed energies [Table S7(supplementary material)].

Increasing the number of maximum angular points in the region relevant for chemical bonding from 434 to 594, while keeping constant the number of radial points (75), the zero point energy decreases $\sim 2 \times 10^{-3}$ hartree, but this decrease is counterbalanced by a similar increase in the total electronic energy of the substance. A further increase of the size of the grid to (99,1280)p has no practical effects. Overall, the net results in terms of static energy on a gram formula weight basis is an increase of 0.45 kJ/mol when passing from the grid (75,434)p to the grid (75,594)p and a further increase of 0.04 kJ/mol when passing from this grid to the grid (99,594)p. Since, we want to calculate later the properties of anhydrous phase-B in an internally consistent way (for reasons discussed in the [Introduction](#)), and it is

particularly demanding in terms of computational costs, we adopted the grid (75,434)p for all calculations. It should be noted that, in any case, the pruned (75,434)p grid spans the radial range as proposed by Gill et al. (1993) with five shells having different angular points. Due to a larger number of radial points and less aggressive pruning, this grid gives more accurate results than the default grid of CRYSTAL (Dovesi et al. 2006).

References

- Akaogi M, Ito E, Navrotsky A (1989) Olivine-modified spinel–spinel transitions in the system Mg_2SiO_4 – Fe_2SiO_4 : calorimetric measurements, thermochemical calculation geophysical application. *J Geophys Res* 94:15671–15686
- Akaogi M, Takayama H, Kojitani H, Kawaji H, Atake T (2007) Low-temperature heat capacities, entropies and enthalpies of Mg_2SiO_4 polymorphs, and α – β – γ and post-spinel phase relations at high pressure. *Phys Chem Miner* 34:169–183
- Anderson OL (1995) Equations of state of solids for geophysics and ceramic science, Oxford monographs on geology and geophysics, N. 21. Oxford University Press, New York
- Anderson OL, Isaak DG, Oda H (1992) High temperature elastic constant data on minerals relevant to geophysics. *Rev Geophys* 30:57–90
- Baur WH (1972) Computer simulated crystal structures of observed and hypothetical Mg_2SiO_4 polymorphs of low and high density. *Am Miner* 57:709–731
- Becke AD (1993) Density-functional thermochemistry. III. The role of exact exchange. *J Chem Phys* 98:5648–5652
- Belov NV, Belova EN, Andrianova NH, Smirnova PF (1951) Determination of the parameters in the olivine (forsterite) structure with the harmonic three-dimensional synthesis. *Dokladi Akademii Nauk SSSR* 81:399–402
- Berman RG (1988) Internally consistent thermodynamic data for minerals in the system Na_2O – K_2O – CaO – MgO – FeO – Fe_2O_3 – Al_2O_3 – SiO_2 – TiO_2 – H_2O – CO_2 . *J Petrol* 29:445–522
- Born M, Huang K (1954) Dynamical theory of crystal lattices. Oxford University Press, Oxford
- Bragg WL, Brown GB (1926) Die Struktur des Olivine. *Zeits Krist* 63:538–556
- Brodholt J, Patel A, Refson K (1996) An ab initio study of the compressional behavior of forsterite. *Am Miner* 76:1100–1109
- Cernik RJ, Murray PK, Pattison P, Fitch AN (1990) A two-circle powder diffractometer for synchrotron radiation with a closed loop encoder feedback system. *J Appl Cryst* 23:292–296
- Chopelas A (1991) Single crystal Raman spectra of forsterite, fayalite and monticellite. *Am Miner* 76:1100–1109
- Chopelas A (2000) Thermal expansivity of mantle relevant magnesium silicates derived from vibrational spectroscopy at high pressure. *Am Miner* 85:270–278
- Chopelas A, Boehler R, Ko T (1994) Thermodynamics and behavior of γ - Mg_2SiO_4 at high pressure: implications for Mg_2SiO_4 phase equilibrium. *Phys Chem Miner* 21:351–359
- Civalleri B, D’Arco P, Orlando R, Saunders VR, Dovesi R (2001) Hartree–Fock geometry optimisation of periodic systems with the CRYSTAL code. *Chem Phys Lett* 348:131
- Cohen RE (1991) Bonding and elasticity of stishovite SiO_2 at high pressure: linearized augmented plane wave calculations. *Am Miner* 76:733–742
- Da Silva C, Stixrude L, Wentzcovitch RM (1997) Elastic anisotropy of forsterite at high pressure. *Geophys Res Lett* 24:1963–1966

- Della Giusta A, Ottonello G, Secco L (1990) Precision estimates of interatomic distances using site occupancies, ionization potentials and polarizability in *Pbnm* silicate olivines. *Acta Cryst B* 46:160–165
- Doll K (2001) Implementation of analytical Hartree–Fock gradients for periodic systems. *Comp Phys Comm* 137:74–88
- Doll K, Harrison NM, Saunders VR (2001) Analytical Hartree–Fock gradients for periodic systems. *Int J Quantum Chem* 82:1–13
- Doll K, Dovesi R, Orlando R (2004) Analytical Hartree–Fock gradients with respect to the cell parameter for systems periodic in three dimensions. *Theor Chem Acc* 112:394–402
- Dovesi R, Saunders VR, Roetti C, Orlando R, Zicovich-Wilson CM, Pascale F, Civalieri B, Doll K, Harrison NM, Bush IJ, D’Arco P, Llunell M (2006) CRYSTAL06 User’s manual, Università di Torino, Torino
- Downs RT, Zha C-S, Duffy TS, Finger LT (1996) The equation of state of forsterite to 17.2 GPa and effects of pressure media. *Am Miner* 81:51–55
- Fei Y, Bertka CM (1999) Phase transitions in the Earth’s mantle and mantle mineralogy. In: Fei Y, Bertka CM, Mysen BO (eds) *Mantle petrology: field observations and high pressure experimentation*, pp 189–207. Special Publication No. 6, Geochemical Society, Houston
- Fei Y, Saxena SK (1986) A thermochemical data base for phase equilibria in the system Fe–Mg–Si–O at high pressure and temperature. *Phys Chem Miner* 13:311–324
- Fei Y, Saxena SK, Navrotsky A (1990) Internally consistent thermodynamic data and equilibrium phase relations for compounds in the system MgO–SiO₂ at high pressure and high temperature. *J Geophys Res* 95:6915–6928
- Fei Y, Mao HK, Shu J, Parthasarathy G, Bassett WA (1992) Simultaneous high-P, high-T X ray diffraction study of β -(Mg, Fe)₂SiO₄ to 26 GPa and 900 K. *J Geophys Res* 97:4489–4495
- Finger LW, Hazen RM, Prewitt CT (1991) Crystal structure of Mg₁₂Si₄O₂₃(OH)₂ (phase B) and Mg₁₄Si₅O₂₄ (phase AnhB). *Am Miner* 76:1–7
- Fujino K, Sasaki S, Takeuchi Y, Sadanaga R (1981) X-ray determination of electron distribution in forsterite, faialite and tephroite. *Acta Cryst B* 37:513–518
- Ganguly J, Frost DJ (2006) Stability of anhydrous phase B: experimental studies and implications for phase relations in subducting slab and the X discontinuity in the mantle. *J Geophys Res* 111:B06203
- Gibbs GV (1982) Molecules as models for bonding in silicates. *Am Miner* 67:421–450
- Gill PMW, Johnson BG, Pople JA (1993) A standard grid for density function calculations. *Chem Phys Lett* 209:506–512
- Guyot F, Wang Y, Gillet P, Ricard Y (1996) Quasi-harmonic computations of thermodynamic parameters of olivines at high-pressure and high-temperature. A comparison with experiment data. *Phys Earth Planet Inter* 98:17–29
- Haiber M, Ballone P, Parrinello M (1997) Structure and dynamics of protonated Mg₂SiO₄: ab-initio molecular dynamics study. *Am Mineral* 82:913–922
- Hazen R (1976) Effect of temperature and pressure on the crystal structure of forsterite. *Am Miner* 61:1280–1293
- Hazen RM, Zhang J, Ko J (1990) Effects of Fe/Mg on the compressibility of synthetic wadsleyite: β -(Mg_{1-x}Fe_x)SiO₄ ($x < 0.25$). *Phys Chem Miner* 17:416–419
- Hazen RM, Downs RT, Finger LW, Ko J (1993) Crystal chemistry of ferromagnesian silicate spinels Evidence of Mg–Si disorder. *Am Miner* 78:1320–1323
- Hazen RM, Weinberger MB, Yang H, Prewitt CT (2000) Comparative high pressure crystal chemistry of wadsleyite, β -(Mg_{1-x}Fe_x)SiO₄, with $x = 0$ and 0.25. *Am Miner* 85:770–777
- Hofmeister A (1987) Single-crystal absorption and reflection infrared spectroscopy of forsterite and fayalite. *Phys Chem Miner* 14:499–513
- Holland TJB, Powell R (1990) An enlarged and updated internally consistent thermodynamic dataset with uncertainties and correlations: the system K₂O–Na₂O–CaO–MgO–MnO–FeO–Fe₂O₃–Al₂O₃–TiO₂–SiO₂–C–H₂–O₂. *J Metamor Geol* 8:89–124
- Horiuchi H, Sawamoto H (1981) β -(Mg,Fe)₂SiO₄: Single crystal X-ray diffraction study. *Am Mineral* 66:568–575
- Iishi K (1978) Lattice dynamics of forsterite. *Am Miner* 63:1198–1208
- Inoue T, Irifune T, Higo Y, Sanchira T, Sueda Y, Yamada A, Shinmei T, Yamazaki D, Ando J, Funakoshi K, Utsumi W (2006) The phase boundary between wadsleyite and ringwoodite in Mg₂SiO₄ determined by in situ X-ray diffraction. *Phys Chem Miner* 33:106–114
- Isaak DG (1991) Elasticity of single crystal forsterite measured to 1700 K. *J Geophys Res* 95:5895–5906
- Isaak DG, Anderson OL, Goto T (1989) Elasticity of single-crystal forsterite measured to 1700 K. *J Geophys Res* 94:5895–5906
- Jackson J, Sinogeikin SV, Bass JD (2000) Sound velocities and elastic properties of γ -Mg₂SiO₄ to 873 K by Brillouin spectroscopy. *Am Miner* 85:296–303
- Jacobs MHG, De Jong BWHS (2003) The high-temperature and high-pressure behavior of MgO derived from lattice vibration calculations. Kieffer’s model revisited. *Phys Chem Chem Phys* 5:2056–2065
- Jacobs MHG, De Jong BWHS (2005) An investigation into thermodynamic consistency of data for the olivine, wadsleyite and ringwoodite form of (Mg, Fe)₂SiO₄. *Geochim Cosmochim Acta* 69:4361–4375
- Jacobs MHG, van der Berg AP, De Jong BWHS (2006) The derivation of thermo-physical properties and phase equilibria of silicate materials from lattice vibrations: application to convection in the Earth’s mantle. *CALPHAD* 30:131–146
- James F, Roos M (1977) MINUIT: a system for function minimisation and analysis of parameters errors and correlation. CERN Computer Center, Geneva, Swiss
- Jochym PT, Parlinski K, Krzywiec P (2004) Elastic tensor of the forsterite (Mg₂SiO₄) under pressure. *Comput Mat Sci* 29:414–418
- Katsura T, Ito E (1989) The system Mg₂SiO₄–Fe₂SiO₄ at high pressures and temperatures: precise determination of stabilities of olivine, modified spinel, and spinel. *J Geophys Res* 94:15,663–15,670
- Katsura T, Yamada H, Nishikawa O, Song MS, Kubo A, Shinmei T, Yokoshi S, Aizawa Y, Yoshino T, Walter MJ, Ito E, Funakoshi K (2004) Olivine-wadsleyite transition in the system (Mg,Fe)₂SiO₄. *J Geophys Res-Solid Earth* 109:B02209
- Kieffer SW (1979a) Thermodynamics and lattice vibrations of minerals: 1. Mineral heat capacities and their relationships to simple lattice vibrational models. *Rev Geophys Space Phys* 17:1–19
- Kieffer SW (1979b) Thermodynamics and lattice vibrations of minerals: 2. Vibrational characteristic of silicates. *Rev Geophys Space Phys* 17:20–34
- Kiefer B, Stixrude L, Wentzcovitch R (1999) Normal and inverse ringwoodite at high pressures. *Am Miner* 84:288–293
- Kiefer B, Stixrude L, Hafner J, Kresse G (2001) Structure and elasticity of wadsleyite at high pressures. *Am Miner* 86:1387–1395
- Kolesov B, Geiger C (2004) A Raman spectroscopic study of Fe–Mg olivines. *Phys Chem Miner* 31:142–154
- Kudoh Y, Takeuchi T (1985) The crystal structure of forsterite Mg₂SiO₄ under high pressure up to 149 kbars. *Zeits Krist* 171:291–302
- Lager GA, Ross FK, Rotella FJ, Jorgensen JD (1981) Neutron powder diffraction of forsterite Mg₂SiO₄: a comparison with single crystal investigations. *J Appl Cryst* 14:137–139

- Lee C, Yang E, Parr RG (1988) Development of the Colle–Salvetti correlation–energy formula into a functional of the electron density. *Phys Rev B* 37:785–789
- Li B, Gwanmesia GD, Liebermann RC (1996) Sound velocities of olivine and beta polymorphs of Mg_2SiO_4 at Earth's transition zone pressures. *Geophys Res Lett* 23:2259–2262
- Li B, Liebermann RC, Weidner D (1998) Elastic moduli of wadsleyite ($\beta\text{-Mg}_2\text{SiO}_4$) to 7 gigapascals and 873 kelvin. *Science* 281:675–677
- Li L, Weidner Wentzcovitch DJ, Da Silva CRS (2007) Vibrational and thermodynamic properties of forsterite at mantle conditions. *J Geophys Res* 112:B05206
- Manghnani MH, Matsui T (1981) Temperature dependence of pressure derivatives of single-crystal elastic constants of pure forsterite (abstract). ISPEI symposium of properties of materials at high pressures and high temperatures, Toronto
- Matsui M (1999) Computer simulation of the Mg_2SiO_4 phases with applications to the 410 seismic discontinuity. *Phys Earth Planet Inter* 116:9–18
- Matsui Y, Manghnani MH (1985) Thermal expansion of single-crystal forsterite to 1023 K by Fizeau interferometry. *Phys Chem Miner* 12:201–210
- Meng Y, Weidner DJ, Gwanmesia DG, Liebermann RC, Vaughan MT, Wang Y, Leinenweber K, Pacalo RE, Yaganeh-Haeri A, Zhao Y (1993) In situ high P – T X Ray diffraction studies on three polymorphs (α , β , γ) of Mg_2SiO_4 . *J Geophys Res* 98:22199–22207
- Meng Y, Fei Y, Weidner D, Gwanmesia GD, Hu J (1994) Hydrostatic compression of $\gamma\text{-Mg}_2\text{SiO}_4$ to mantle pressures and 700 K: thermal equation of state and related thermodynamic properties. *Phys Chem Miner* 21:407–412
- Ming LC, Manghnani MH, Kim YH, Usha-Devi S, Xu JA, Ito E (1992) Thermal expansion studies of $(\text{Mg}, \text{Fe})_2\text{SiO}_4$ -spinel using synchrotron radiation. In: Saxena SK (ed) Thermodynamic data, systematics and estimation. *Advances in Physical Geochemistry*, vol 10. Springer, New York
- Moore PB, Smith JV (1970) Crystal structure of $\beta\text{-Mg}_2\text{SiO}_4$: crystal-chemical and geophysical implications. *Phys Earth Planet Inter* 3:166–177
- Nada R, Nicholas JB, McCarthy MI, Hess AC (1996) Basis sets for ab initio periodic Hartree–Fock studies of zeolite/adsorbate interactions: He, Ne, and Ar in silica sodalite. *Int J Quantum Chem* 60:809
- Noel Y, Catti M, Ph D'Arco, Dovesi R (2006) The vibrational frequencies of forsterite Mg_2SiO_4 : an all-electron ab-initio study with the CRYSTAL code. *Phys Chem Miner* 33:383–393
- Otonello G, Civalleri B, Vetuschi Zuccolini M, Zicovich Wilson CM (2007) Ab-initio thermal physics and Cr-isotopic fractionation of MgCr_2O_4 . *Am Miner* 92:98–108
- Pascale F, Zicovich-Wilson CM, Lopez-Gejo F, Civalleri B, Orlando R, Dovesi R (2004a) The calculation of the vibrational frequencies of crystalline compounds and its implementation in the CRYSTAL code. *J Comput Chem* 25:888–897
- Pascale F, Zicovich-Wilson CM, Orlando R, Roetti C, Ugliengo P, Dovesi R (2004b) Vibration frequencies of $\text{Mg}_3\text{Al}_2\text{Si}_3\text{O}_{12}$ pyrope. An ab initio study with the CRYSTAL code. *J Phys Chem B* 109:6146–6152
- Piekarz P, Jochym PT, Parlinski K, Lazewski J (2002) High-pressure and thermal properties of $\gamma\text{-Mg}_2\text{SiO}_4$ from first-principles calculations. *J Chem Phys* 117:3340–3344
- Ridgen SM, Jackson I (1991) Elasticity of germanate and silicate spinels at high pressure. *J Geophys Res* 96:9999–10006
- Robie RA, Hemingway BS, Fisher JR (1978) Thermodynamic properties of minerals and related substances at 298.15 K and 1 bar (10^5 Pascals) pressure and at higher temperatures. USGS Bull, 1452, 456 pp
- Robie RA, Hemingway BS, Takei H (1982) Heat capacities and entropies of Mg_2SiO_4 , Mn_2SiO_4 , and Co_2SiO_4 between 5 and 380 K. *Am Miner* 67:470–482
- Sawamoto H, Weidner DJ, Sasaki S, Kumazawa M (1984) Single-crystal elastic properties of the modified spinel (beta) phase of Mg_2SiO_4 . *Science* 224:749–751
- Saxena S, Chatterjee N, Fei Y, Shen G (1993) Thermodynamic data of oxides and silicates. Springer, Berlin
- Schlegel HB (1982) Optimization of equilibrium geometries and transition structures. *J Comput Chem* 3:214–218
- Scott AP, Radom L (1996) Harmonic vibrational frequencies: an evaluation of Hartree–Fock, Møller–Plesset, quadratic configuration interaction, density functional theory, and semiempirical scale factors. *J Phys Chem* 100:16502–16513
- Servoin JL, Piriou B (1973) Infrared reflectivity and Raman scattering of magnesium silicate single crystal. *Phys Status Solidi B* 55:677–686
- Smyth JR, Hazen RM (1973) The crystal structure of forsterite and hortonolite at several temperatures up to 900°C. *Am Miner* 58:588–593
- Stephens PJ, Devlin FJ, Chabalowski CF, Frisch MJ (1994) Ab initio calculation of vibrational absorption and circular dichroism spectra using density functional force fields. *J Phys Chem* 98(45):11623–11627
- Sumino Y, Anderson OL (1984) Elastic constants of minerals. In: Carmichael RS (ed) CRC handbook of physical properties of rocks. CRC Press, Boca Raton
- Sumino Y, Nishizawa O, Goto T, Ohno I, Ozima I (1977) Temperature variation of elastic constants of single crystal forsterite between 190 and 400°C. *J Phys Earth* 28:273–280
- Suzuki I, Ohtani E, Kumazawa M (1979) Thermal expansion of $\gamma\text{-Mg}_2\text{SiO}_4$. *J Phys Earth* 27:53–61
- Suzuki I, Ohtani E, Kumazawa M (1980) Thermal expansion of modified spinel $\beta\text{-Mg}_2\text{SiO}_4$. *J Phys Earth* 28:273–280
- Tanaka S, Sawamoto H, Fujimura A, Akamatsu T, Hashizume H, Shimomura O (1987) Precise measurement of compressibility of $\beta\text{-Mg}_2\text{SiO}_4$ using synchrotron radiation. Paper presented at 28th high pressure conference, Japan, Kobe
- Van der Wal RJ, Vos A, Kirfel A (1987) Conflicting results for the deformation properties of Forsterite, Mg_2SiO_4 . *Acta Cryst* 43:132–143
- Watanabe H (1982) Thermochemical properties of synthetic high-pressure compounds relevant to the Earth's mantle. In: Akimoto H, Manghnani MH (eds) High pressure research in geophysics. Center for Academic Publications, Tokyo, pp 441–464
- Weidner DJ, Sawamoto H, Sasaki S, Kumazawa M (1984) Single-crystal elastic properties of the spinel phase of Mg_2SiO_4 . *J Geophys Res* 89:7852–7860
- Wentzcovitch RM, Martins JL, Prize GD (1993) Ab initio molecular dynamics with variable cell shape: application to MgSiO_3 -perovskite. *Phys Rev Lett* 70:3947–3950
- Wu Z, Wentzcovitch RM (2007) Vibrational and thermodynamic properties of wadsleyite: a density functional study. *J Geophys Res* (in press)
- Yoneda A (1990) Pressure derivatives and elastic constants of single crystal MgO and MgAl_2O_4 . *J Phys Earth* 38:19–55
- Yu YG, Wentzcovitch RM (2006) Density functional study of vibrational and thermodynamic properties of ringwoodite. *J Geophys Res* 111:B12202
- Zha CS, Duffy TS, Downs RT, Mao HK, Hemley RJ (1996) Sound velocity and elasticity of single-crystal forsterite to 16 GPa. *J Geophys Res* 101:17535–17545